Journal of Marine Research, 63, 529–561, 2005

Mixing within the interior of the Faeroe-Shetland Channel

by Phil Hosegood[1,2], Hans van Haren[1] and Cornelis Veth[1]

ABSTRACT

Observations of the distribution of the density field, the dissipation rate of turbulent kinetic energy, ε, the vertical diffusivity, K_z, and optical backscatter over a repeated cross-section of the Faeroe-Shetland Channel (FSC) are presented within the context of ocean mixing. Turbulence in the permanent pycnocline occurs in discrete vertical patches of thickness 20–50 m coincident with layers of elevated vertical current shear magnitude, $|\mathbf{S}| > 10^{-2}\ \mathrm{s}^{-1}$. The layers of elevated shear result from high-wavenumber internal waves which may break through shear instabilities as indicated by critical Richardson numbers, $Ri < 1$. The internal waves are ubiquitous features of strong boundary currents flowing along continental shelves and are likely generated here by geostrophic adjustment of the pycnocline in response to lateral excursions of the boundary current over the Shetland slope or by the scattering of internal tide energy. The pycnocline as a whole exhibits $K_z > 10^{-4.5}\ \mathrm{m}^2\ \mathrm{s}^{-1}$, a factor of ~3 larger than typical open ocean thermoclines but still implying a weak exchange of water mass properties across the density interface despite the confined and isolated patches of enhanced turbulence which elevate K_z by an order of magnitude. Both the boundary current and the deep interior are typified by weak stratification and locally high $K_z \approx 10^{-3}\ \mathrm{m}^2\ \mathrm{s}^{-1}$, but low turbulent buoyancy fluxes. The strongest observed turbulence and mixing in the channel, $\varepsilon = O(10^{-7}\ \mathrm{W\ kg}^{-1})$ and $K_z > 10^{-3}\ \mathrm{m}^2\ \mathrm{s}^{-1}$ respectively, is observed in the near-bed region over the Shetland slope and results from solibore propagation up the slope and the asymmetric response of the bottom boundary layer to the tidal currents. The overall contribution of the FSC to oceanic mixing would appear to be about half of the required canonical value of $K_z = 10^{-4}\ \mathrm{m}^2\ \mathrm{s}^{-1}$ given the observed short duration and/or infrequent occurrence of the processes generating turbulence in the near-bed region, the spatially confined sporadic mixing patches in the pycnocline, and the low turbulent buoyancy fluxes in the interior and slope current.

1. Introduction

The Faeroe-Shetland Channel (FSC) is a dynamic and energetic hydrographic environment. A persistent slope current, intensified by the converging topography north of the Wyville-Thomson Ridge (WTR) (Huthnance, 1986; Saunders, 1990), flows in a poleward direction along the Shetland slope, transporting 3 Sv of Atlantic water, and the majority of the heat, to the Nordic Seas (Sherwin *et al.,* 1999). The jet-like and localized nature of the current, in which velocities exceed 1 m s^{-1} (Hopkins, 1999), inherently implies large

1. Royal Netherlands Institute of Sea Research (NIOZ), P.O. Box 59, 1790 AB Den Burg, The Netherlands.
2. Present address: Applied Physics Laboratory, University of Washington, 1013 NE 40th Street, Seattle, Washington, 98105, U.S.A. ***email: hosegood@apl.washington.edu***

current shears whilst meanders and deflections may arise as a result of instabilities of the slope current. Eddies subsequently formed have a periodicity of approximately 14 days and propagate along the Shetland slope, apparently attached to the 800 m isobath (Sherwin *et al.,* 1999). Eddies may also be generated by the intense shears produced by the merging of the warm Atlantic waters with the cold Nordic waters in the southern region of the FSC (Oey, 1998), purportedly with an associated vacillation of the slope current and a periodicity of 5–10 days. Sherwin (1988) reports the existence of a deep internal tide in the southern region of the FSC generated by the barotropic tidal flow across the WTR, whilst the combination of stratification and bottom slope along the FSC further enable the possibility of internal tide generation. Atmospheric forcing may generate continental shelf waves (CSW) in the FSC with quasi-steady or periodic barotropic responses depending on the intensity and duration of the wind (Gordon and Huthnance, 1987), the currents being confined to the Shetland side of the slope and decaying exponentially offshore.

In this paper we investigate mixing within the FSC during the project Processes over the Continental Slope (PROCS). Mixing in the interior of the FSC is important because the channel represents a major conduit for warm Atlantic waters flowing northward at the surface above a permanent pycnocline with a return southward flow of cold water beneath it; thus the degree of mixing that occurs in the channel interior, and particularly across the pycnocline that separates the water masses, has consequences for the properties of the respective water masses and subsequently for the large-scale thermohaline circulation. It was previously established that the near-bed region over the slope in the channel is subject to turbulent mixing due to convective instabilities resulting from the asymmetric response of the bottom boundary layer to tidal flows (Hosegood and van Haren, 2003). Enhanced mixing and sediment transport was also shown to occur due to the propagation of internal bores up the slope (Hosegood *et al.,* 2004; Hosegood and van Haren, 2004). However, the degree of mixing within the channel and its internal variability, both temporal and spatial, has not been addressed, whether due to dynamic processes in the interior itself or due to boundary processes which transmit their effects into the interior (e.g. Thorpe, 1999). The focusing of internal waves following their repeated reflection from the boundaries of a confined basin (Maas *et al.,* 1997) was considered to be a mechanism that could potentially promote enhanced mixing due to the semi-enclosed shape of the channel.

The potential of similar hydrographically dynamic and geometrically constrained channels in elevating oceanic mixing rates has been considered elsewhere. Observations across the Florida Current in the Straits of Florida revealed five mixing regimes which were characterized by the contrasting level and composition of shear which drives the mixing (Winkel *et al.,* 2002). The interior was dominated by shear fluctuations 1–4 times stronger than the open ocean, resulting in moderate diffusivities. The high velocity core of the current, similar to the slope current in the FSC in terms of volume transport but with slightly larger current speeds ($>1.6\ \mathrm{m\ s^{-1}}$ compared to $\leq 1\ \mathrm{m\ s^{-1}}$ in the FSC), was characterized by low diffusivities and weak shear fluctuations whilst intermittent features beneath the core exhibited strong turbulence and mixing. Intermittent features attributed to

alternating layers of enhanced shear were also observed beneath the Kuroshio (which is not constrained in a semi-enclosed basin like the FSC or Florida Straits) and are proposed by Rainville and Pinkel (2004) to be common features of strong currents riding along continental shelves. Near to the sloping sides of the Florida Straits, finescale shear is predominantly cross-isobath and results in a widely varying intensity of turbulence. Turbulent stratified boundary layers in which turbulence and stratification are enhanced above levels of the surrounding waters and are typically located immediately above the homogenous bottom boundary layer, carry 1 Sv within 100 m of the channel floor and account for nearly half of the section-averaged diffusivity. A significant difference between the Florida Straits and the FSC, however, is the flow reversal below the permanent pycnocline, accompanied by inherently high mean shear, in the current study region with poleward flow above and equatorward flow beneath as opposed to the unidirectional, poleward-directed Florida current occupying the entire channel. Furthermore, the tidal regime in the FSC has a strong influence on the hydrodynamics, intensifying and retarding the predominantly along-isobath currents over the slope on a semidiurnal timescale and potentially generating an internal tide over the Shetland slope where the permanent pycnocline intersects the boundary.

A number of transects were conducted during PROCS across an entire transect of the FSC. Vertical profiles of temperature, salinity, light transmission and velocity microstructure were taken, allowing us the opportunity to consider the large-scale density distribution within the channel and to identify regions of enhanced turbulence and turbidity especially in the interior and also at the boundaries. Long-Ranger Acoustic Doppler Current Profilers (LR-ADCP) moored at the sea bed at intermediate positions over the slope permit insight into the role played by large-scale vertical current shear in enhancing turbulent dissipation rates. We relate regions of enhanced turbulent dissipation rates to the large scale stratification and the distribution of optical scatterers and assess the importance of shear-induced mixing in the interior as opposed to the boundary mixing previously observed in the region.

The paper is organized as follows; in the following section we outline the study region and the instrumentation employed, whilst in Section 3 the results are presented. The vertical structure of the water column at two positions over the slope is considered in terms of stratification, shear and turbulence. Results from vertical profiles taken during transects conducted across the entire channel are then presented. In Section 4 we discuss our results from the perspective of the mixing regimes within the FSC and potential role played by varying background conditions before conclusions are drawn in Section 5.

2. Study area and methods

a. PROCS and the Faeroe-Shetland Channel

The principal aim of Processes over the Continental Slope (PROCS) is the study of internal wave-related mixing processes in the Faeroe-Shetland Channel (FSC) and their

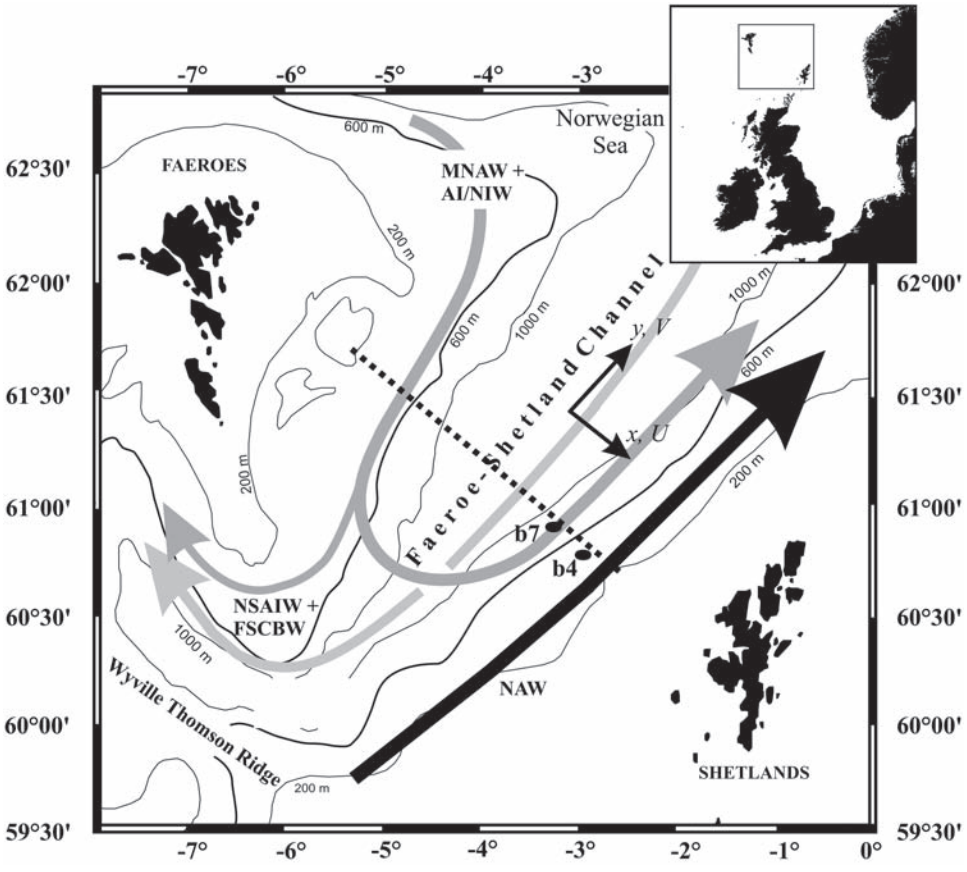

Figure 1. Map of study region indicating the position of the two Long-Ranger ADCPs, b4 and b7, at 600 m and 800 m depth respectively. Co-ordinate axes are defined for cross-slope and long-slope directions as shown. The transect along which the vertical profiles were taken is indicated by the dashed black line.

impact on the distribution of sediment and benthic fauna in the near-bed region. The FSC is a semi-enclosed basin located to the north of Scotland and running in a principally northeast/southwest direction (Fig. 1) with an approximate distance of 175 km between the shelf breaks on either side of the channel. Topography is relatively smooth, with slopes between 1000 m and 450 m of 0.01–0.02 radians on the Shetland side. Surface roughness is negligible compared to the lengthscales required to generate internal waves; seismic reflection profiles in the study region reveal the presence of sheetform drifts with smooth surfaces and covered by a thin sandy contourite layer (Howe *et al.,* 2002) between 600–800 m depths and which is responsible for the convex shape of the slope. The large-scale circulation (see Turrell *et al.* (1999) for details) consists of a northeasterly surface flow above the permanent pycnocline, found between depths of 400–600 m, and a

deep return flow to the southwest below. Surface flow over the Shetland slope is dominated by the slope current, whose warm and saline core (~9°C, >35.3 PSU, 27.45 kg m^{-3}) is typically found at a depth of ~200 m in water of depth ~400–800 m.

Two cruises were carried out during the field study, PROCS-1 between 14th April–5th May 1999 (Yearday, $t = 103–124$), and PROCS-2 between 21st September–13th October 1999 ($t = 263–285$). Whilst a number of moorings sampling current speed, temperature and sediment fluxes were deployed at the sea bed during both cruises, the emphasis in this paper is on the results from instruments employed during a total of four transects (numbered sequentially as T1, T2, T3 and T4) conducted across the channel and over the Shetland slope, in addition to data from LR-ADCPs deployed at the sea bed on the Shetland slope. T1 ($t = 109.78 \rightarrow 112.68$) and T2 ($t = 116.09 \rightarrow 119.35$) spanned the entire channel during the PROCS-1 whilst during PROCS-2 one short transect (T3, $t = 271.34 \rightarrow 272.33$) over the Shetland slope and one complete transect (T4, $t = 277.15 \rightarrow 278.83$) were completed.

b. Conditions during transects

The observations presented here are neither truly synoptic nor necessarily representative of mean background conditions. Complete transects took three days to complete. Whilst it is beyond the scope of the present paper to relate the observed mixing to specific nonsteady motions which vary in time and space throughout the channel, we highlight three specific processes that were active during the sampling program and would be expected to influence the measurements.

i. Atmospheric storms. The FSC lies in a region subject to frequent and severe wind forcing arising from the passage of atmospheric depressions. During both cruises low pressure systems passed to within varying degrees of proximity to the study region and have the potential to either directly mix the surface mixed layer by mechanical mixing or to force large-scale motions (e.g. continental shelf waves as modeled by Gordon and Huthnance, 1987) whose currents indirectly drive mixing processes. However, as will be shown in the following sections, there are observable differences between transects conducted during the same cruises and which may be related to specific storms. Atmospheric storms, during which wind speed exceeded 20 m s^{-1} as measured by the RV *Pelagia,* passed directly through the study region on days 110 (PROCS-1) and 275 (PROCS-2). Therefore transects T1 (PROCS-1) and T4 (PROCS-2) were conducted <2 days after severe storms (more details of the storm during PROCS-1 are given in Hosegood and van Haren, 2004).

ii. Internal tides. Enhanced shear and turbulence observed over slopes and nearby in the interior (e.g. Moum *et al.,* 2002) are frequently ascribed to the reflection and/or breaking of internal tides which have been generated at locations where the bottom slope, γ, matches that of the internal tide characteristic, dz/dx. In the ocean interior enhanced turbulence

along rays inclined to the vertical has been interpreted as evidence of the effects of internal tide propagation (Pingree and New, 1991; Lueck and Mudge, 1997; Lien and Gregg, 2001). The slope, dz/dx, of a linear internal wave ray of frequency σ propagating through a two-dimensional (neglecting the long-isobath component of propagation) continuously stratified fluid is given by;

$$\frac{dz}{dx} = \left(\frac{\sigma^2 - f^2}{N^2 - \sigma^2}\right)^{1/2}, \tag{1}$$

(e.g. Prinsenberg *et al.,* 1974) where f is the Coriolis parameter and N^2 is the square of the buoyancy frequency N;

$$N^2 = -\frac{g}{\rho_o}\frac{\Delta\rho}{\Delta z}, \tag{2}$$

where g is the acceleration due to gravity, ρ_o is a reference potential density and $\Delta\rho$ is the change in local density over a vertical distance Δz. The effects of horizontal velocity and density gradients may modify (1) as;

$$\frac{dz}{dx} = \pm\left(\frac{N_x^2 \pm \{N_x^4 + [\sigma^2 - f(f + \partial_x V)](N^2 - \sigma^2)\}^{1/2}}{(N^2 - \sigma^2)}\right)^{1/2}, \tag{3}$$

(Mooers, 1973), where $N_x^2 = -(g/\rho_o)\partial\rho/\partial x$ is the scaled horizontal density gradient and $\partial_x V = \partial V/\partial x$ is the cross-isobath gradient of the mean long-isobath velocity component. The time-mean (over the period of the cruises) of the horizontal density gradient at 500 m depth where the density gradients are largest is $O(0.1\ \mathrm{kg\ m^{-3}})$ over a distance of approximately 10 km, giving $N_x^2 = O(10^{-7})\ \mathrm{s^{-2}}$. The time-mean of the horizontal velocity gradient at the same depth between the two LR-ADCP moorings is 13 cm $\mathrm{s^{-1}}$, over 10 km, corresponding to $\partial_x V = O(10^{-5}\ \mathrm{s^{-1}}) \approx 0.1f$. Both terms are of sufficiently small magnitude as to be insignificant in altering the characteristic of the M_2 internal tide, particularly within the context of the temporal variability of the stratification throughout the channel as a whole and which will have a much more profound effect on the path of the internal tide than the influence of $\partial_x V$ and N_x^2.

The characteristics for internal tide rays at the lunar semidiurnal (M_2) tidal frequency, $\sigma_{M2} = 1.405 \times 10^{-4}\ \mathrm{s^{-1}}$, are computed assuming generation at the Shetland slope where the bottom slope, $\gamma = dz/dx$. Two ray-paths are calculated for each transect, originating at the shallowest and deepest positions over the slope where the stratification during the transect facilitates critical conditions for the M_2 internal tide. The slope, dz/dx, is calculated at horizontal intervals of approximately 3 km across the channel toward the Faeroes with the angle on reflection at the surface and the bottom maintained with respect to the vertical; such a procedure is no more than an approximate estimate given the unknown influence of scattering processes on reflection and broadening of the beam due to the dissipation throughout its propagation (e.g. Pingree and New, 1991). We are also

unable to take into account the temporal variability in N and assume the measured density field to remain constant throughout the period of the CTD cross-section.

iii. Near-bed solibores. Earlier observations have indicated the passage of 'solibores' up the Shetland slope, taking the form of internal bores and/or trains of solitary internal waves depending on the stage of evolution at which the feature was sampled (Hosegood and van Haren, 2004; Hosegood *et al.,* 2004). Of the transects conducted during PROCS, only T1 coincided with the occurrence of a solibore over the Shetland slope and which is clearly evident in the data presented here whilst T2 is indicative of conditions just prior to the up-slope surge that is characteristic of the feature. The solibores appear to occur with a subinertial periodicity of approximately four days and to facilitate greatly enhanced near-bed mixing and elevated vertical current shear across the strongly stratified density interface on which the waves are formed. The intense near-bed stratification and its variability in position over the slope during the passage of the solibore will therefore strongly affect the possibility of internal tide generation which is intimately dependent on the stratification. Massive sediment resuspension also occurs, with sediment fluxes remaining high up to three days after the passage of the solibore.

c. Data handling

The Conductivity-Temperature-Depth (CTD) system employed is a Seabird 911 *plus* model with a sampling rate of 24 Hz. The purpose of the CTD is two-fold; firstly as a means of resolving the density field within the channel and, secondly, as a means of calculating the vertical scale of density overturns from which the degree of turbulent mixing may be inferred (See Appendix 1). The density field is represented by N^2. Its relationship with the magnitude of the vertical current shear, $\mathbf{S} = (\Delta u/\Delta z,\ \Delta v/\Delta z)$ calculated as;

$$|\mathbf{S}| = \sqrt{\left(\frac{\Delta u}{\Delta z}\right)^2 + \left(\frac{\Delta v}{\Delta z}\right)^2}, \tag{4}$$

where u and v are the cross-isobath and long-isobath current components respectively and $\Delta z = 4$ m is the vertical distance over which the shear and density is determined, defines the stability of the water column to vertical shear and is represented by the local Richardson number, Ri;

$$Ri = \frac{N^2}{|\mathbf{S}|^2}. \tag{5}$$

In a linear system $Ri < 0.25$ is a necessary condition for instabilities to occur due to small disturbances whilst for nonlinear 3-D systems in which the perturbations are not small $Ri < 1$ is sufficient for instability to occur (Miles, 1987). Horizontal current velocities were measured by RDI Long Ranger Acoustic Doppler Current Profilers (LR-ADCP)

moored over the Shetland slope at depths of 600 m and 800 m during each cruise. Data were obtained between heights above the bed, z, of approximately 15–415 m (corresponding to a depth range of 190–590 m and 385–785 m) at $\Delta z = 4$ m vertical intervals and with a sampling interval of 5 minutes.

Estimates of the rate of dissipation of turbulent kinetic energy, ε, were made by the FLY II microstructure profiler. Details of the estimation of ε from the turbulent shear data are given in Appendix 2. FLY casts were made immediately following the CTD casts and reached to within 5 m of the sea bed or to its maximum depth rating of 1000 m. The diapycnal diffusivity is then computed as;

$$K_z = \Gamma_o \frac{\varepsilon}{N^2}, \tag{6}$$

(Osborn, 1980). The mixing efficiency, Γ_o, is taken here as the constant value of 0.2 as derived from laboratory experiments (Rohr and van Atta, 1987), but is often considered to be dependent on the age of the mixing event (e.g. Smyth *et al.,* 2001). In oceanic observations, Γ_o may range from 0.05 (Yamazaki and Osborn, 1993) to 0.7 (Gargett and Moum, 1995).

Estimates of optical backscatter were made using a Seapoint STM optical backscatter sensor (OBS) mounted on the CTD frame. Optical backscatter indicates the presence of suspended particulate matter (SPM), referred to as turbidity, with the limitation that the raw signal (measured in Volts with a higher voltage indicating a greater proportion of suspended particles) depends heavily on the particle size in accordance with Bunt *et al.* (1999) who found that optical devices are most sensitive to particles <20 μm in diameter.

3. Results

a. Vertical distribution of $|\boldsymbol{S}|^2$, N^2 and ε over the slope

Current velocity measurements are unavailable for the entire transects but the mooring of 2 LR-ADCPs over the Shetland slope allows an assessment of the role played by shear in facilitating mixing throughout a large portion of the water column in that specific region. The horizontal distance between some of the FLY casts and ADCPs was <1 km which is significant on the space-time scales of internal waves but close enough for the discrimination of flow regimes that are not solely governed by internal wave dynamics. The emphasis here therefore is not to relate specific instances of shear instability to enhanced ε but to characterize portions of the water column in terms of $|\mathbf{S}|^2$, N^2 and ε which can then be used to interpret the ε profiles from the other parts of the channel where no current velocity data are available.

Over the Shetland slope at the location of the ADCP at 600 m depth, $N^2 < 10^{-6}\ \mathrm{s}^{-2}$ above 300 m depth toward the surface and is accompanied by low ε, corresponding to the position of the slope current core (C) as determined by the current speeds measured by the ADCP (Fig. 2a). The relatively shallow depth and position of the slope current means that

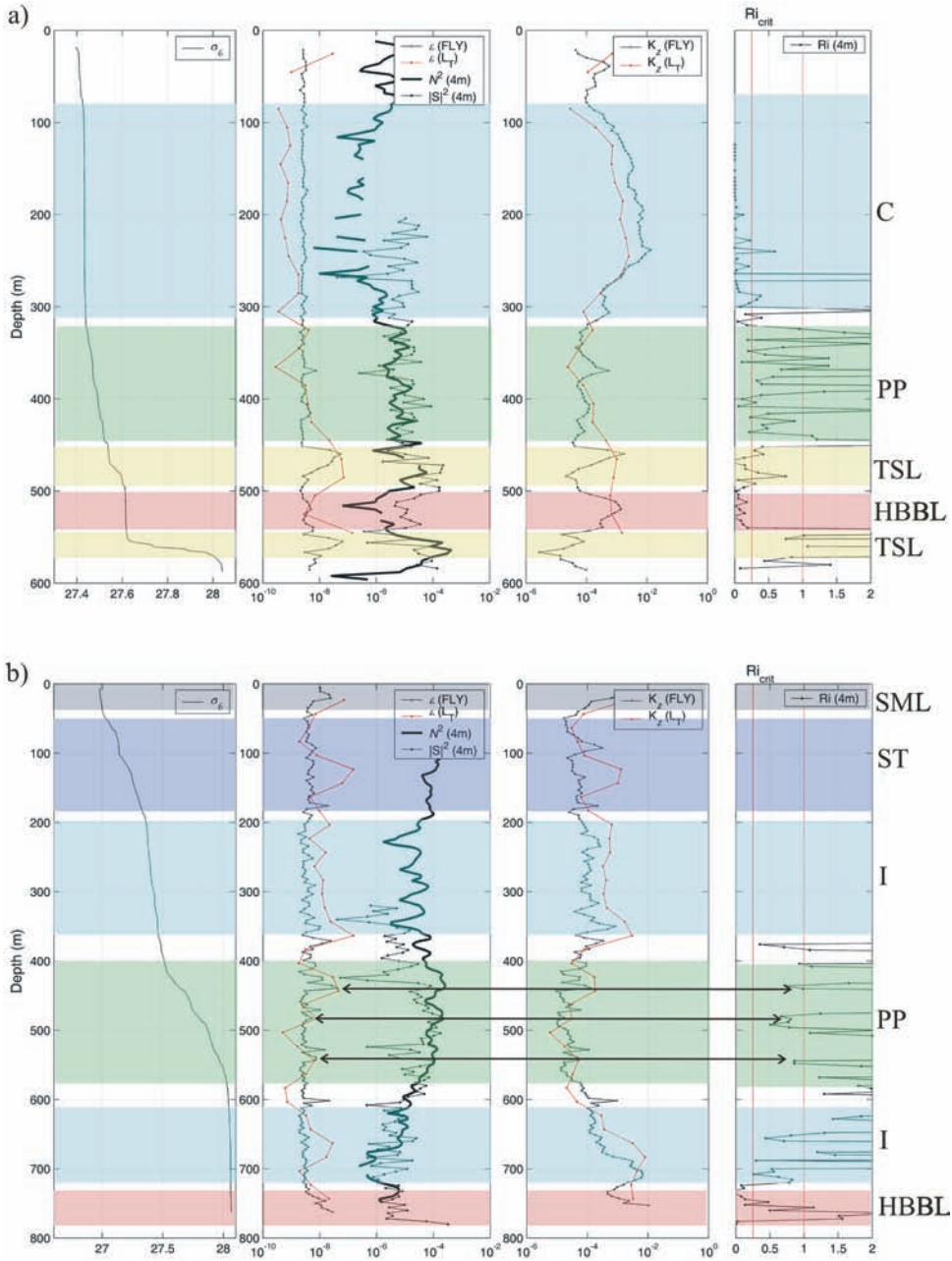

Figure 2. Profiles during (a) Station 98 ($t = 116.71$) at 1b4 and (b) Station 79 ($t = 277.58$) of (i) potential density (σ_θ) in kg m^{-3}, (ii) ε (W kg^{-1}) calculated from microstructure measurements according to Eq. 8. (FLY) and from CTD profiles (L_T), buoyancy frequency, N^2 (s^{-2}) and vertical shear magnitude, $|\mathbf{S}|^2$ (s^{-2}), (iii) vertical diffusivity, K_z (m^2 s^{-1}) derived from estimates of ε using direct and indirect methods, and (iv) Richardson numbers calculated over $z = 4$ m. Gaps in the N^2 profiles correspond to regions of unstable stratification. Shaded regions correspond to homogenous bottom boundary layers (HBBL), turbulent stratified layers (TSL), interior (I), permanent pycnocline (PP), surface mixed layer (SML) and slope current core (C), and are labelled accordingly on the right-hand side of the figures.

the remainder of the water column is divided into the upper portion of the permanent pycnocline (PP) (the lower portion having been incorporated into the boundary layers) in which N^2 and $|\mathbf{S}|^2$ are both relatively constant and of $O(10^{-5}\ \mathrm{s}^{-2})$, and the bottom boundary layers. A delicate balance is maintained in the PP in which conditions for shear instability, $Ri < 1$ for flows which depart from the assumption of linearity, are sporadically achieved and result in the observed turbulent patches. The near-bed region exhibits complicated structure due to the periodic passing of the PP. Occurring on subinertial timescales, solibores surge up the slope creating a turbulent stratified layer (TSL) near to the bed (<50 m height above the bed) but which, depending on the prior conditions, do so *beneath* the original homogenous bottom boundary layer (HBBL). TSL is arbitrarily defined as a layer in which $\varepsilon > 10^{-8}\ \mathrm{W\ kg}^{-1}$ and $N^2 > 10^{-5}\ \mathrm{s}^{-2}$ but how they appear in observations is strongly influenced by the nature and stage of the process that generates the enhanced turbulence. We expect that the stratification supports strong shear which at a point in time destabilizes the fluid leading to Kelvin-Helmholtz-type instabilities and, eventually, turbulence. As the mixing progresses, the stratification is reduced such that observations made toward the end of the process may reveal weaker stratification than would previously have been observed whilst turbulence remains high. Such a case is illustrated in Figure 2a, where the solibore is evident as an intrusion of dense fluid ($0.4\ \mathrm{kg\ m}^{-3}$ denser than the overlying fluid) from lower down the slope bounded above by strong $N^2 > 10^{-4}\ \mathrm{s}^{-2}$ and $|\mathbf{S}|^2$ and a distinctly turbulent layer where $\varepsilon = 6.5 \times 10^{-8}\ \mathrm{W\ kg}^{-1}$. We interpret the weakly stratified region between 500–550 m depth as the remnants of the HBBL which extended to the bottom prior to the solibore. A second TSL is found above the HBBL in the same manner as Winkel *et al.* (2002), distinct as a being more stratified and sheared than the underlying water, and turbulent to the same degree as the lowest TSL. Note that the upper portion of the turbulent patch is actually weakly stratified implying that the layer has been subject to mixing over a period of time prior to the CTD and FLY casts.

In 800 m water depth during PROCS-3 (Fig. 2b), the profile conducted after the storm indicates a more typical partioning of the water column. A surface mixed layer (SML) occupies the upper 50 m, below which the establishment of the seasonal thermocline (ST) is evident as a strongly stratified region of $N^2 > 10^{-4}\ \mathrm{s}^{-2}$. Between 200 m and 350 m is the interior, lying between the strongly stratified seasonal thermocline (ST) and PP, and characterized by $N^2 = O(10^{-5}\ \mathrm{s}^{-2})$ and $\varepsilon < 10^{-8}\ \mathrm{W\ kg}^{-1}$. Within the PP the strong stratification generally maintains $Ri > 1$ except for specific patches of vertical extent ≈20 m. A good degree of correlation exists for regions with $Ri < 1$ with enhanced ε (see arrows in Fig. 2b) although as noted above, and particularly pertinent to the permanent pycnocline where the stratification is expected to support comparatively small-scale internal waves, caution must be exercised in attributing specific turbulent patches to instances of shear instability inferred from Figure 2. Below the PP extends a region typical of the deep interior within the channel, with $|\mathbf{S}|^2$, N^2 and ε of similar magnitudes to the

interior portion above the PP in the same profiles. A thin HBBL of thickness <30 m is present in which $\varepsilon > 10^{-8}$ W kg^{-1}.

b. Spatial distribution of stratification, turbulence and turbidity within the channel

i. Stratification. The intensity of the stratification in the PP varies across the channel from $10^{-4.5} > N^2 > 10^{-5}$ s^{-2} in the central channel but reaches $N^2 = O(10^{-4}$ s$^{-2})$ toward the slopes (Fig. 3). The consequence of the reduction in N^2 away from the channel boundaries is that the bandwidth of the internal wave band, defined as $f < \sigma < N$, $N \gg f$, is reduced with smaller N^2; thus high frequency internal waves are unsupported toward regions of reduced stratification, i.e. toward the interior, and may therefore break or be reflected back (LeBlond and Mysak, 1978). The depth of the PP exhibits a marked asymmetry across the channel during T1 and T2, intersecting the slope at a typical depth of 500 m on the Shetland side, but reaching the top of the Faeroe slope at a depth of approximately 250 m and doming toward the surface in the middle of the channel. The asymmetry is consistent with the geostrophic control of the poleward-flowing slope current over the Shetland slope which results in a sloping of the isopycnals downward toward the slope, i.e. lighter water on the right-hand side in the direction of flow in the northern hemisphere. Modified North Atlantic water flows in the opposite direction to the slope current, i.e. southward, along the Faeroe slope before turning at the Wyville-Thomson Ridge to join the northward-flowing slope current (Turrell *et al.,* 1999). Thus the sloping isopycnals on the Faeroe side of the channel are also consistent with the geostrophic balance of a southward-flowing current.

HBBLs are noticeable over both the Shetland and the Faeroe slopes. Values of $N^2 < 10^{-6}$ s^{-2} are typical in the lowest ~50 m of the water column but density inversions at the bed are often evident (white shading in Fig. 3). Over the slope at depths of 300–700 m (i.e. in the vicinity of where the PP impinges on the slope) the stratification increases abruptly above the HBBLs to $N^2 > 10^{-5}$ s^{-2}, suggestive of the presence of TSLs as observed in the individual profiles of Figure 2. The deep interior (I), defined as below the 0°C isotherm, is weakly stratified ($N^2 < 10^{-6}$ s^{-2}) in all transects with $N^2 < 10^{-7}$ s^{-2} found at the foot of the slopes on occasions.

The stratification during PROCS-3 is different to the first cruise in that an ST is observed at a depth of 100 m where $10^{-5} < N^2 < 10^{-4}$ s^{-2} (Fig. 3c, d). As a result there is a greatly reduced upper interior region of weak stratification. Stratification is also further enhanced throughout the PP to $N^2 > 10^{-4.5}$ s^{-2}.

During both cruises the core of the slope current (C) over the Shetland slope is notable as a region of weak stratification; during T1 $N^2 = O(10^{-8}$ s$^{-2})$ above the ADCP moored at 600 m depth and is only an order of magnitude larger during T2. Its location during T3, T4 is less obvious but is implied by the position of the 9°C isotherm during the latter transect to be a region of relatively weak stratification over the slope.

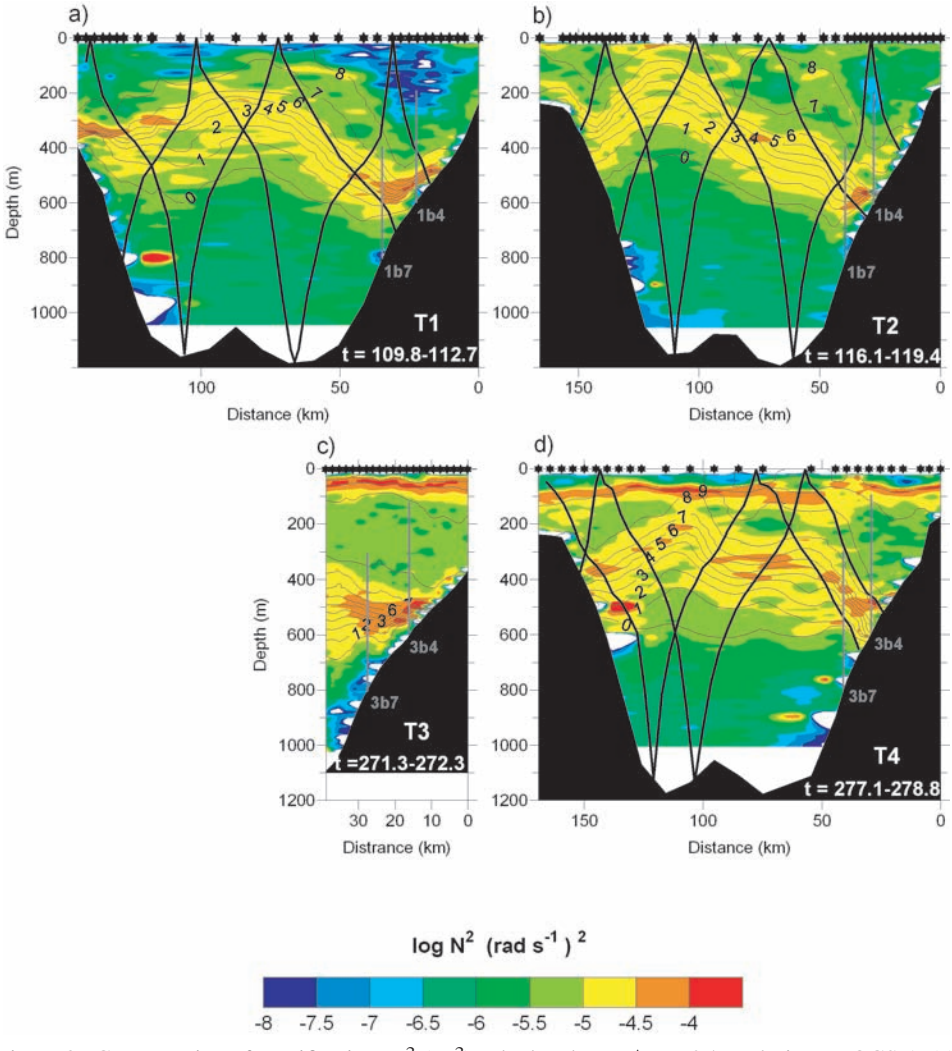

Figure 3. Cross-section of stratification, N^2 (s^{-2}) calculated over $\Delta z = 25$ m, during PROCS-1; (a) T1, (b) T2, and during PROCS-2; (c) T3 and (d) T4. Positions of the two LR-ADCPs are indicated at depths of 600 m (*b4) and 800 m (*b7) over the Shetland slope. Isotherms measured by the CTD are indicated and the internal tide characteristics assuming generation at the Shetland slope and upward propagation into the interior are indicated as the thick black lines.

ii. Turbulent dissipation and vertical diffusivity. Cross-sections of the rate of dissipation of turbulent kinetic energy, ε (Fig. 4), computed using the FLY data and of diapycnal diffusivity, K_z (Fig. 5), indicate the highest ε to be immediately over the Shetland slope in the HBBL and TSLs and at the surface in the SML. During T1 in PROCS-1, $\varepsilon = O(10^{-7}\ \mathrm{W\ kg^{-1}})$ in the region where the PP intersects the slope, with large diapycnal

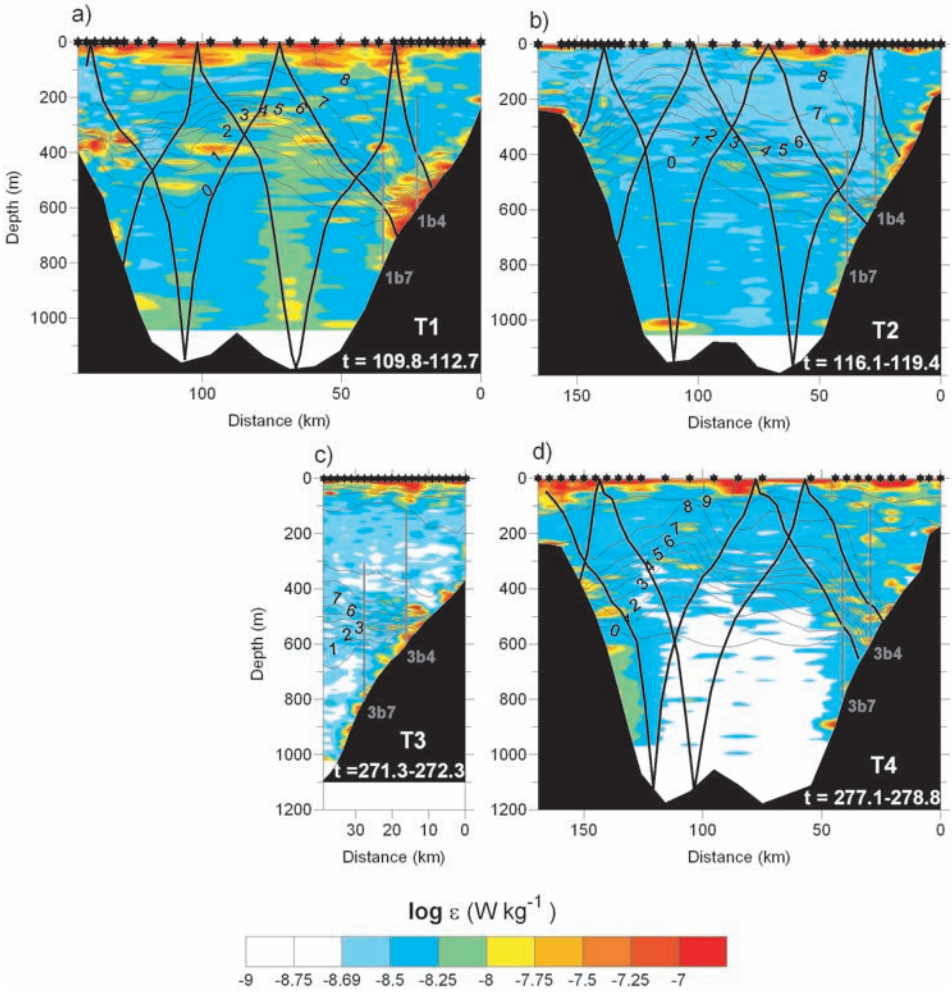

Figure 4. As for Figure 3 but for the rate of dissipation of turbulent kinetic energy, ε (W kg^{-1}) estimated from the FLY.

diffusivities $O(10^{-2}$ m^2 s$^{-1})$ found in the weakly stratified fluid immediately below it. This is due to the passage of a 'solibore' up the slope at the time of the transect (Hosegood and van Haren, 2004). Both ε and K_z are also elevated adjacent to the Faeroe slope but in a more confined region constrained to the top of the slope where the PP intersects or passes over the top of, the slope. The weak stratification in the deep interior (I) results in values of $K_z = O(10^{-2}$ m^2 s$^{-1})$ during both T1 and T2. Whilst measurements of ε near the surface may be dominated by turbulence generated by breaking surface waves, the elevated levels of K_z at a distance of ≈50 km from the Shetland slope during T1 extend to a depth of 300 m which is beyond the direct influence of surface waves. These high values of K_z are

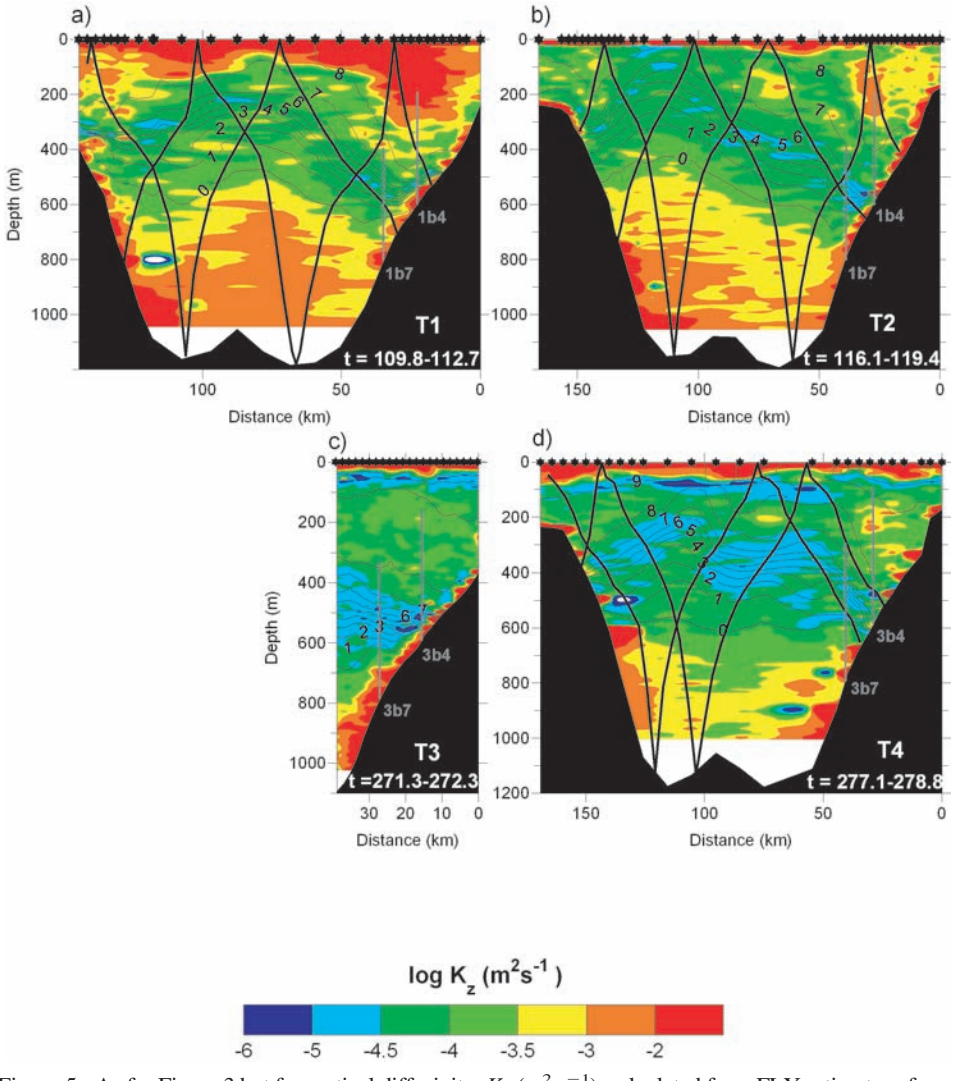

Figure 5. As for Figure 3 but for vertical diffusivity, K_Z (m^2 s^{-1}), calculated from FLY estimates of ε.

due to the low values of N^2 within the slope current and are evident again to a lesser extent during T2 approximately 10 km to the east and where there is now no elevated ε. Sporadic turbulent patches are evident in the PP and often exceed $10^{-7.5}$ W kg^{-1} during T1. T2 exhibits considerably lower ε and K_z compared to T1, particularly in the HBBL/TSL over the Shetland slope where the strongest turbulence was observed during T1.

During PROCS-3 ε and K_z are lower in the channel interior during T3 and T4 (Figs. 4, 5c, d) than in T1 but are comparable to T2. The short but intensive transect (stations every 1 km) over the Shetland slope, T3, indicates a turbulent HBBL of vertical extent <50 m

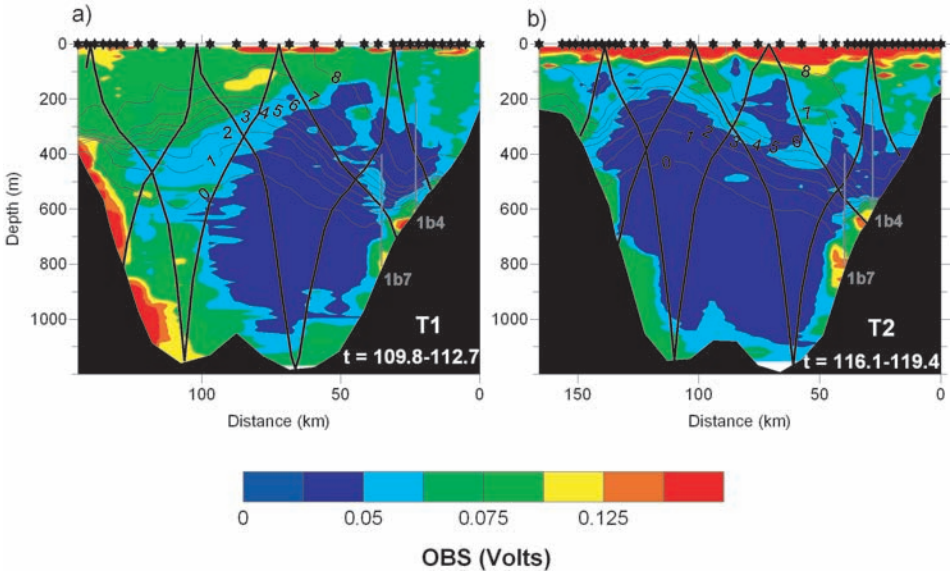

Figure 6. Optical backscatter, OBS (Volts; uncalibrated units), during PROCS-1; (a) T1 and (b) T2.

where $\varepsilon > 10^{-8}$ W kg^{-1} (Fig. 4c), reaching $O(10^{-7}$ W kg$^{-1})$ where the pycnocline intersects the slope. At this location $K_z = O(10^{-5}$ m^2 s$^{-1})$ away from the HBBL but is sporadically reduced to 10^{-6} m^2 s^{-1} in strongly stratified patches, whilst the weak stratification at greater depth facilitates $K_z > 10^{-3}$ m^2 s^{-1} near the boundary (Fig. 5c). Dissipation is enhanced to $O(10^{-8}$ W kg$^{-1})$ at a depth of 600–1000 m over the Faeroe slope (Fig. 4d) during T4 whilst observed $\varepsilon = O(10^{-7}$ W kg$^{-1})$ at the surface across the entire channel is most likely due to breaking surface waves generated by the passage of a storm just prior to the transect in a similar manner to observations during T1. During both cruises diffusivities exceed $K_z = O(10^{-4}$ m^2 s$^{-1})$ in the slope current over the Shetland slope, reaching 10^{-3} m^2 s^{-1} during T4 when ε is elevated in patches over a broad region inshore of the 9°C isotherm. The deep interior (I) is quiescent during T4, with ε at the noise level of the FLY and K_z artificially high by up to an order of magnitude.

iii. Turbidity. The OBS mounted on the CTD frame indicates a region of enhanced turbidity on the Shetland slope during both T1 and T2 at a depth of 600–900 m (Fig. 6). In both cases there are two distinct cores of maximum turbidity, both of which are situated beneath the PP and are separated by a region of comparatively weaker turbidity. The close horizontal spacing of stations over the slope ensures that the two cores are not simply a relic of sparse sampling and that they occur on either side of a 'knee' in the slope formed as a result of contourite deposits at a depth of approximately 700 m on the Shetland slope (Howe *et al.,* 2002). The lateral extent of the turbid cores is <5 km but values are elevated beyond those in the interior up to 10 km from the boundary. During T1, and to a lesser

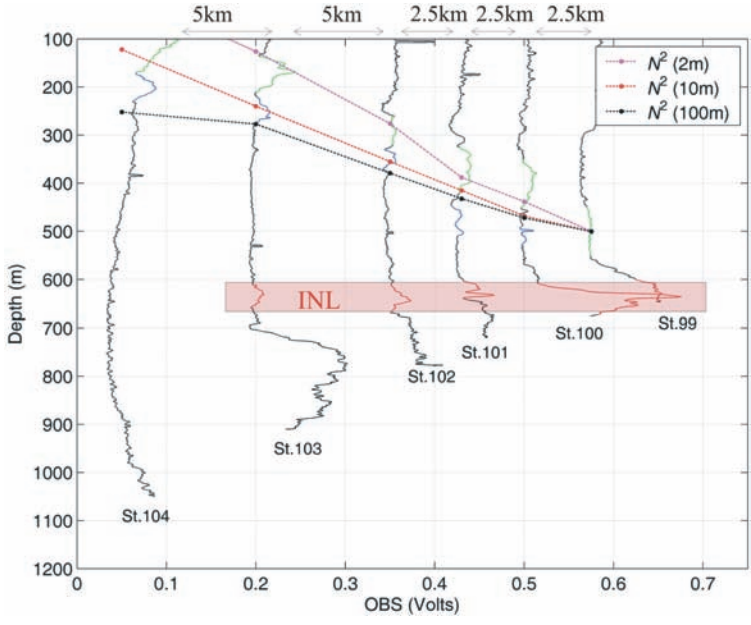

Figure 7. Vertical profiles of optical backscatter (OBS) at Stations 100–104 during T2. Each profile is offset to be proportional to the spacing between stations. The midwater patches of enhanced OBS values are coloured green and blue, with the green parts indicating the upper portion of the patch and the blue part the lower portion; it is not clear if they both relate to the same patch or are distinct from each other. The internal tide characteristics are plotted for N^2 calculated with different values of Δz, with the mean of N^2 within the green portion of the profile used in the application of Eq. 4. The INL is indicated by the highlighted red portion of each profile—note the absence of the INL at Station 104. The distance between stations is indicated at the top of the figure.

degree during T2, the entire Faeroe slope exhibits strong turbidity in a thin layer above the sea bed, with elevated turbidity extending >50 km into the interior. As expected, the lowest turbidity is found in the center of the channel but extends upward from the deep interior into and across the PP.

During T2 distinct levels of elevated turbidity are evident at midwater depths of approximately 650 m at stations in water depths ranging from 670–918 m (Fig. 7) and represent evidence of intermediate nepheloid layers (INLs). The INL originates from the Shetland slope at Station 99 in a water depth of 650 m where vigorous mixing is often observed due to the impinging of the permanent pycnocline on the slope in the form of solibores (Hosegood and van Haren, 2004) and extends out to Station 103 at which point the water depth is 918 m, thus maintaining its signature over a lateral distance of 12.5 km. The INL ceases to be detectable in the OBS profile at Station 104, a farther 5 km offshore. On detaching from the sea bed at Station 100, the INL spreads along a surface of constant density, corresponding to the 28.0 $\pm$ 0.06 kg m^{-3} isopycnal surface.

A distinct band of elevated turbidity extends upward and away and from the Shetland slope into the interior of the channel during T1, originating at a depth of 600–700 m which is approximately that of the deepest internal tidal characteristics originating at the slope. The angle of inclination of the turbidity band is similar, but slightly less steep, to that predicted for the internal tide by (1); we may expect that the angle of the internal tide characteristics may further steepen toward that of the turbidity band with a reduction in N in the region near the slope which is observed during T2. During T2 similar regions of elevated optical backscatter are observed in band-like structures but which appear not to emanate from the slope, although again in regions through which the internal tide characteristics are predicted to pass. The characteristics are thus plotted for six locations over the Shetland slope during T2 for which enhanced patches of turbidity of typical vertical extent of 75 m are evident at decreasing depths offshore (Fig. 7). The slope of the characteristics determined from (1) may be seen to vary depending on the vertical distance, Δz, over which N^2 is calculated, with the smaller increments resulting in a steeper slope. It is necessary to account for variations in dz/dx due to varying N given our lack of knowledge of the true spatial scale that is relevant to an internal tide in the region, essentially the scale over which the internal tide 'feels' the stratification. The location of the patches of enhanced turbidity relates well to the predicted path of the internal tide over a range of values of Δz, with the $\Delta z = 2$ m beam giving the best fit, and implies that the elevated turbidity may be related to the generation and propagation of an internal tide from the Shetland slope at a depth of around 500 m. The patches are observed in water of distinctly different density and thus not attributable to advection along isopycnal surfaces. Their signature is observed up to a horizontal distance of 17.5 km from the slope after which it merges with the surface region of enhanced turbidity.

4. Discussion

a. Mixing regimes in the Faeroe-Shetland Channel

In the broadest sense the FSC may be divided into homogenous boundary layers characterized by low N^2 and high ε and K_z, the weakly stratified interior in which K_z is high due to low N^2, and the strongly stratified permanent pycnocline where ε is sporadically elevated in confined patches. As stated in the introduction however, the FSC is a dynamic environment and such a generalization understates the complexity and spatial variability in mixing regimes in the channel. Surface mixed layers (SML) result primarily from surface forcing, with turbulent mixing arising from, amongst other processes, breaking surface waves and convective overturning. Homogenous, or very weakly stratified, bottom boundary layers (HBBL) over the slopes are subject to a multitude of mixing processes, not least the asymmetric response of the bottom boundary layer to the along-isobath tidal flows which subsequently leads to convective instabilities and turbulent bursting (Hosegood and van Haren, 2003) and the propagation of solibores up the Shetland slope (Hosegood and van Haren, 2004). The latter process, evident in T1, results in $\varepsilon >$

10^{-7} W kg^{-1} concentrated in a thin layer of approximately 50 m vertical extent above the bed. In a similar manner Winkel *et al.* (2002) report a vigorous event within a 20-m mixed layer over the east channel wall in the Florida Straits and whose high dissipation exceeds the predictions of internal wave scaling. Despite being unable to establish the cause of the enhanced mixing, the vigorous turbulence there was in stark contrast to profiles conducted seven days earlier and indicated the temporal variability in turbulence intensity in the vicinity of the sloping boundaries observed in the Florida Straits and which we also observed here in the FSC. ε varies by up to two orders of magnitude over the Shetland slope between T1 and T2 conducted four days later and reflects the difficulty in assessing the contribution of boundary layers to mixing processes throughout the channel as a whole given an imperfect knowledge of the processes that govern the dynamics of the boundary layers and their temporal variability.

Turbulent stratified layers (TSL) as noted by Winkel *et al.* (2002) are not obvious in the data from transects presented here because of their limited vertical extent but are more noticeable when individual profiles are considered. They appear to be limited to regions over the sloping sides of the channel and are found atop of the HBBLs and on either side of the PP as the increase in stratification is outweighed by an accompanying elevation in $|\mathbf{S}|^2$. $Ri < 1$ typically and implies that TSLs are generated in response to the formation Kelvin-Helmholtz billows rather than the convective instabilities that have been shown to characterize the HBBL (Hosegood and van Haren, 2003). The mixing in the TSLs appears to be controlled by marginal internal wave stability (van Haren *et al.,* 1999), whereby the mean background shear supported by the stratification in the PP interacts with high frequency (breaking) internal waves to periodically lower Ri to values required for shear instability.

The turbulent patches observed in the PP may, on the basis of the observations presented here, also be attributed to shear instabilities. Figure 8 indicates the ε profiles conducted at the locations of the LR-ADCPs from which it is clear that the turbulent patches in the PP tend to coincide with regions of high $|\mathbf{S}|^2$ between depths of 400–600 m. The maximum shear is concentrated in distinct layers of vertical thickness 20–50 m in which $|\mathbf{S}|^2 > 10^{-4}\ s^{-2}$ frequently. The vertical extent of the shear layers is commensurate with those observed by Alford and Pinkel (2000), but who conclude that a high strain rate is a better indicator of internal wave breaking than the shear. The layers are also similar in intensity and size to those observed by Rainville and Pinkel (2004) below the Kuroshio, and who suggest the layers are attributable to internal waves whose generation is associated with the presence of the boundary current. In the present case of the FSC internal waves may be generated by, amongst various processes, the geostrophic adjustment of the PP in response to changes in the position and intensity of the boundary current which will see a corresponding change in the density field, specifically the slope of the PP toward the Shetland slope. Systems having undergone geostrophic adjustment possess less energy in their end states than they do initially (Kuo and Polvani, 1997) due to the dispersal of energy in pulses of Poincaré waves (Cahn, 1945). A definitive evaluation of the generation

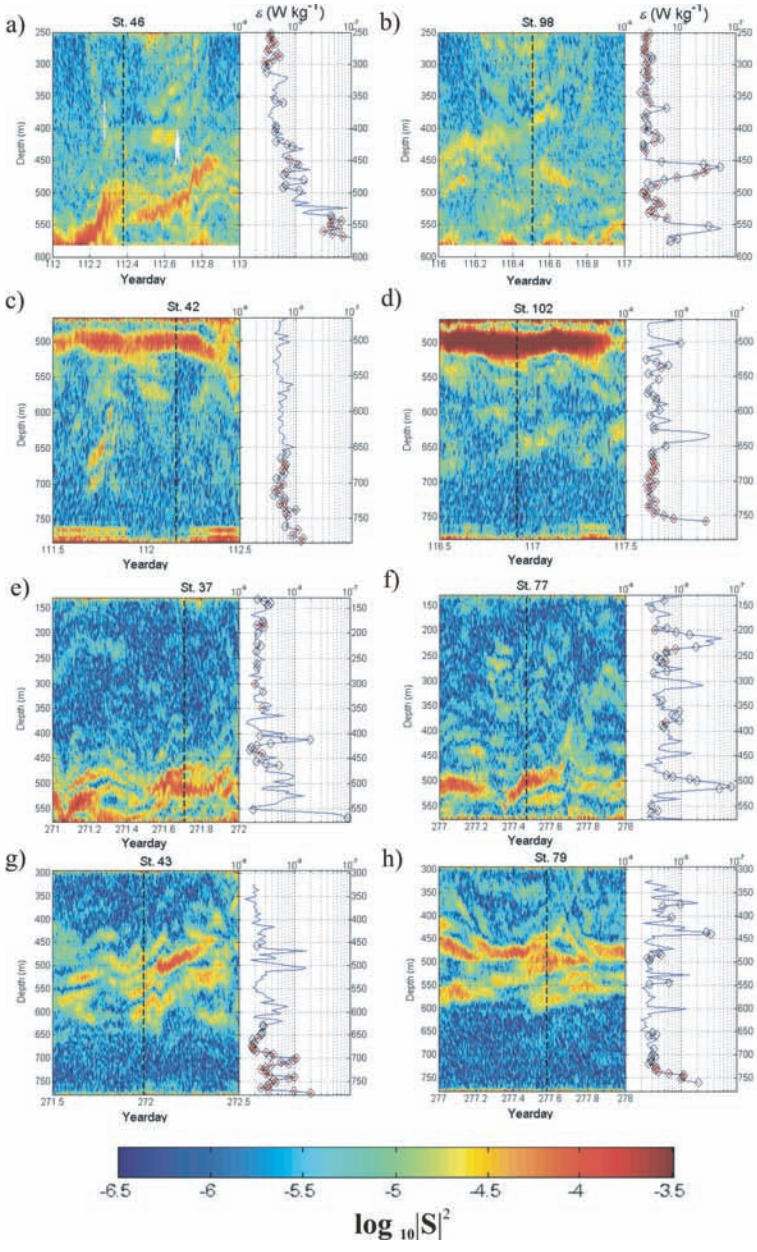

Figure 8. $|\mathbf{S}|^2$ (s^{-2}) calculated over $\Delta z = 4$ m for stations over the Shetland slope during PROCS-1 (a–d) and PROCS-2 (e–h) at the location of the two LR-ADCPs at 600 m and 800 m depth and the corresponding profiles of ε (W kg^{-1}) from the FLY. Black diamonds on the ε profiles indicate $Ri < 1$ and the red dots $Ri < 0.25$. The times of the profiles are indicated as the black dashed lines overlying the plots of $|\mathbf{S}|^2$.

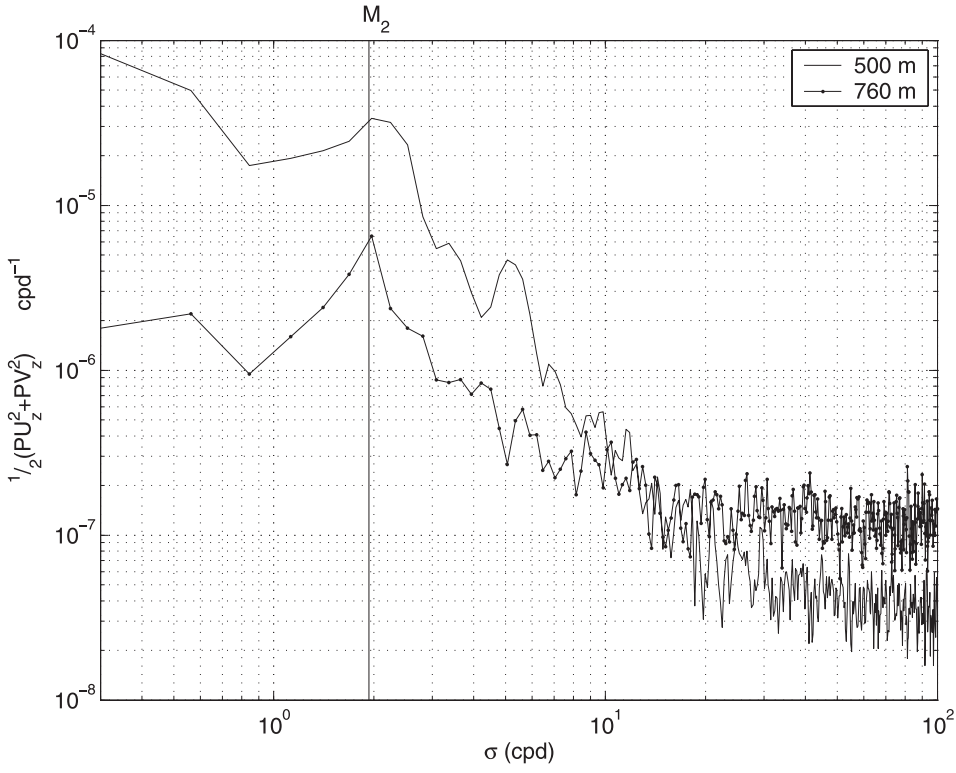

Figure 9. Shear spectra, ½ ($PU_zU_z + PV_zV_z$) ($\Delta z = 4$ m) at depths of 500 m and 760 m from LR-ADCP in water of depth 800 m during PROCS-1. The two spectra correspond to the position of the permanent pycnocline (500 m) and to the near-bed region (760 m) and have been normalized with the respective N^2 at each depth, $N^2_{500} = 50$ cpd, $N^2_{760} = 10$ cpd.

mechanism is however beyond the scope of the current paper but warrants further consideration. Shear spectra from depths of 500 m and 760 m measured at 1b7 (800 m depth), corresponding to the PP and the near-bed region respectively, indicate a broader and more energetic internal wave band in the PP, with shear variance a factor ~5 higher than near the bed (Fig. 9). This indicates the importance of internal wave-induced shear in the PP as the source of the observed turbulent patches, whilst in contrast the distinct peak at the M_2 semidiurnal tidal frequency toward the bed implies the importance of a tidally-driven, frictionally sheared bottom boundary layer as a means of generating the observed near-bed turbulence. These observations, both in terms of spectral energy levels and slopes, are similar to measured shear spectra in the central North Sea at the depths of the major thermocline and near the sea-bed (van Haren, 2000). The smearing of energy across the semidiurnal frequency band ($1.83 < \sigma < 2.01$ cpd) in the PP is indicative of the interaction of tidal motions with the varying background conditions (van Haren, 2004).

The discrepancy between the timing and location of turbulent patches with critical *Ri*

may be attributed to the distance between the ADCP profiles and the FLY profiles such that there is likely to be a small time lag in the observations between a measured region of $|\mathbf{S}|^2$ sampled by the ADCP and the turbulent patch measured by the FLY. The decay time-scale of turbulence in a stratified shear flow without a persistent energy source is 1/10–1/6 of a buoyancy period, N_T (Crawford, 1986). Thus, in the absence of a continuous energy source we would expect the turbulent patches in the pycnocline to decay within a timescale of approximately 3–5 minutes given $N_T = 30$ minutes based on the observed stratification. From Figure 8 however, we can see that the layers of large $|\mathbf{S}|^2$, which represent the energy source for the turbulent patches, typically persist for timescales on the order of hours. The patches subsequently generated may thus be expected to persist for a comparable timescale on the assumption that the shear is supported by stratification and which the mixing is eroding. Outside the high mean shear region towards the edges of the pycnocline more sporadic patches of relatively weaker shear, $10^{-5} < |\mathbf{S}|^2 < 10^{-4}\ \mathrm{s}^{-2}$, occur, most likely associated with breaking internal waves, and the turbulent patches that subsequently result will not persist for a considerable length of time. Here the weaker shear is able to lower Ri to critical levels due to the lower N^2.

The core of the slope current over the Shetland slope is a region of high diffusivity but in which the buoyancy flux, $J_B = -K_z N^2$, is low. The current core is a homogenous water mass with the θ-S characteristics of warm, saline North Atlantic Water (Turrell *et al.,* 1999). This is in contrast to observations made across the Florida Current, where the *weakest* diffusivities were observed in the current core due to the combination of low dissipation rates and high stratification (Winkel *et al.,* 2002). In both geographical contexts the vertical shear associated with the current cores result in sloping isopycnals in the correct sense for thermal wind balance; in the FSC this has implications for the position of the pycnocline over the Shetland slope. Whilst the data presented here describe a quasi-synoptic overview of the mixing patterns within the FSC, the effects of slope current meanders and eddies described in the Introduction propagating along the Shetland slope will undoubtedly modulate the behaviour of the slope current core and thus the PP in the vicinity of the slope. As previously mentioned this may have implications for internal wave generation through the geostrophic adjustment of the PP in response to lateral movements of the slope current core.

b. The influence of background conditions on mixing

The transects conducted following the storms on days 112 and 277 exhibited higher levels of turbulence throughout the whole channel than the transects conducted either several days later (day 116) or several days before (day 271) (Fig. 10), suggesting that the storms may have been responsible for energising the internal wave field above background conditions across a broad frequency range. The direct influence of wind-induced mixing would not be expected to penetrate below $O(100\ \mathrm{m})$, whilst waves generated by the passage of a strong atmospheric disturbance may generate internal waves that penetrate

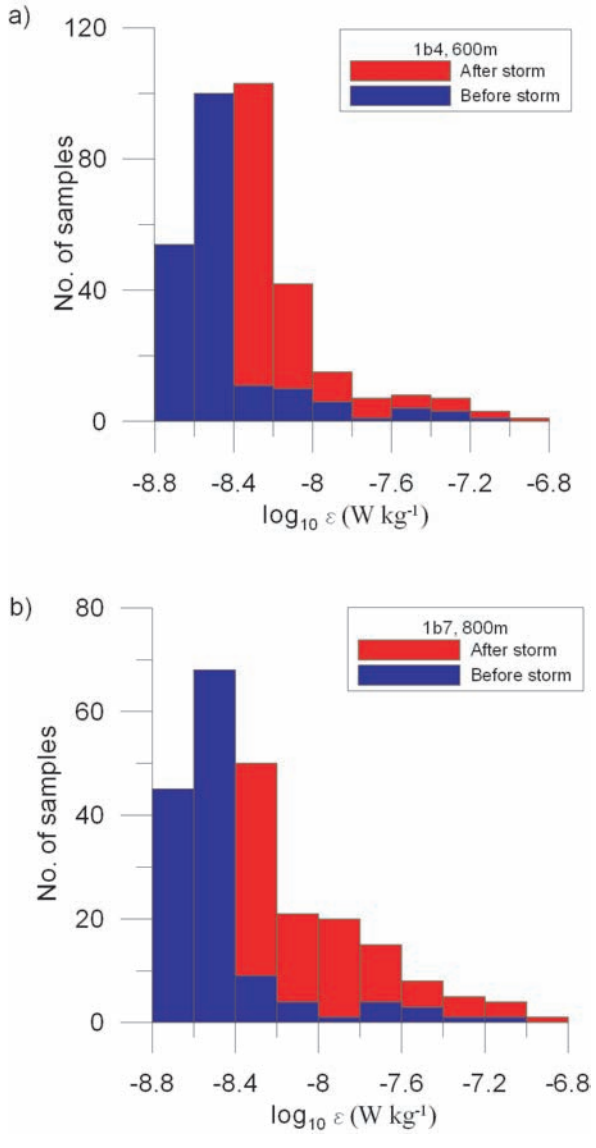

Figure 10. Number of samples (i.e. approximately 1 metre bins) per $\log_{10}$ 0.2 bin of ε, before (blue) and after (red) the storm during PROCS-1 at (a) 1b4 in 600 m water depth, and (b) at 1b7 in 800 m water depth.

downwards into the ocean interior (e.g. Thorpe, 1975; Garrett and Munk, 1979). There is no evidence of enhanced $|\mathbf{S}|^2$ during the profiles conducted after the storm however (Figs. 8a, c, f, h) compared to those conducted before or long after when the storm's influence would have dissipated and it is unclear to what extent, if at all, the storm indeed elevated

turbulence throughout the FSC. It is possible that the shear was of a spatial scale that was not resolvable by the ADCP. The consistent absence of a spectral peak at the local inertial frequency, f, would appear to preclude the forcing of internal waves by inertial waves. Alford and Pinkel (2000) suggest that mixing events off the coast of California which are characterized by high effective strain rate, $|\partial\hat{w}/\partial z|$, and high Ri are suggestive of convective overturning rather than shear instabilities. This is a possibility for explaining the enhanced ε observed after storms but which cannot be tested here due to insufficient resolution of the ADCP.

As seen in Figure 7, the characteristics of the internal tide are sensitive to the choice of Δz when calculating N^2 whilst the temporal and spatial variability of the density field of which we have an imperfect knowledge is almost certain to cause a departure of the beam paths from that when assuming steady state, constant background stratification. Thus whilst there is no evidence of distinct beams of enhanced dissipation emanating from the Shetland slope which would be suggestive of focused internal tide propagation, there are nonetheless aspects of the distribution of ε which are suggestive of internal tides playing a role in promoting mixing in the channel.

A linear internal tide generation model (Gerkema, 2001) predicts the tidally averaged energy density and baroclinic cross-isobath velocities arising from the generation of an internal tide over the Shetland slope (Fig. 11). The uniformity of N^2 in the cross-channel direction in the model realistically invalidates a direct comparison of the results of the model with the observations presented here but the model does indicate the lack of an oceanward propagating beam of internal tidal energy emanating from the slope and the broken, unfocussed web of enhanced baroclinic velocities and energy density. The web results from the scattering upon reflection of internal tidal energy into smaller scale internal waves whose random superposition throughout the channel locally enhances vertical current shear and increases the likelihood of internal wave breaking and thus elevated turbulent dissipation rates. Whilst coherent patterns are generally sought as evidence of the presence of the internal tide it is clear that, in contrast to the focusing of energy predicted by Maas *et al.* (1997) for specific geometries, the unfocused distribution of energy in the FSC will lead to sporadic patches of enhanced current velocities. It is noted however that the regions of enhanced energy density and baroclinic velocity predicted by the model coincide well with the predicted location of the surface reflection of the internal tide computed from the observations. Thus whilst there is no clear evidence of the effects of the internal tide in the FSC promoting mixing through shear instabilities, the model suggests that such effects will manifest themselves as isolated patches of turbulent activity as observed in the PP in the observations and possibly enhanced energy towards the surface where the internal tide reflects.

The apparent similarity between the band of increased turbidity above the Shetland slope and the predicted path of the internal tidal ray is suggestive of the internal tide generating a preferred pathway for the transport of suspended particulate matter (SPM). The definitive

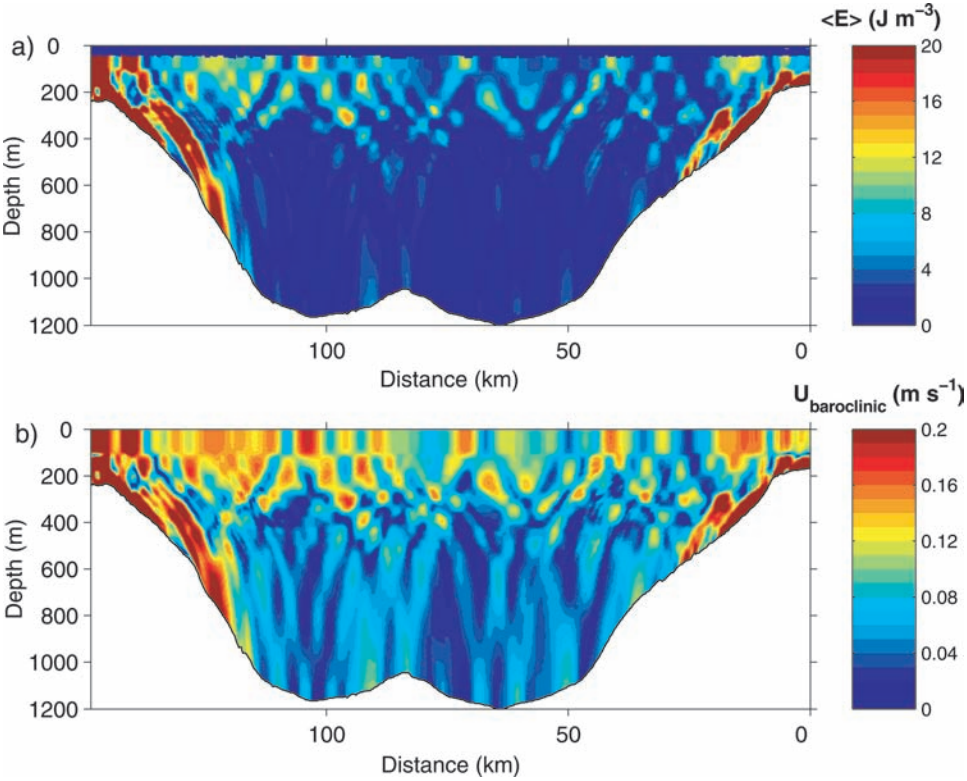

Figure 11. (a) Tidal averaged energy density, $\langle E \rangle$ (J m^{-3}), and (b) baroclinic cross-slope velocity, $U_{baroclinic}$ (m s^{-1}) predicted by a linear internal tide generation model (Gerkema, 2001) for the Faeroe Shetland Channel. Stratification is taken from the observed profile taken at a mid-channel station and is constant in the cross-channel direction. The model is run for 10 tidal cycles with σ = 1.9324 cpd = M_2. The predicted internal tide characteristics from T1 are overlain over the model results.

identification of a link between the two processes is hindered however by the widely differing timescales associated with the problem and our inability in the current study to determine the origin of the SPM, specifically whether it is settling out under the action of gravity from above or whether it is being transported upwards along the path of the IT following resuspension at the Shetland slope. Typical sediment settling rates are O(20 mm s^{-1}), equivalent to approximately 20 m per day during which two semidiurnal tidal cycles have been completed, such that the patterns of turbidity observed here would have to be almost permanently present given their spatial extent in the presence of velocity and density fields which are subject to variations at tidal timescales. The internal tide may sufficiently weaken vertical density gradients along its characteristics to encourage SPM to settle through the *locally* weakly stratified region. Such local changes in stratification may not be resolved by the current sampling strategy. The advection of SPM along isopycnals

in a three-dimensional frame of reference may also be important given their inclination downwards towards the slope. Again the quasi-synoptic nature of the observations prohibits a definitive evaluation of the link because we cannot ascertain with any certainty the temporal evolution of the density field over the Shetland slope at timescales of less than the 4 days between transects. The observed variability of the isopycnals between transects and the previously established current intensity in the mean flow certainly suggests however that the advection of SPM by the mean currents along the steeply sloping isopycnals may explain the presence of the turbidity filaments.

c. Implications for large-scale mixing

The large values of $K_z > 10^{-4}\ \mathrm{m^2\,s^{-1}}$ observed in the deeper part (>600 m) of the channel (Fig. 5) have little impact of the redistribution of water mass properties across the permanent pycnocline but do nonetheless represent significantly higher diffusivities than the canonical open ocean value of $10^{-5}\ \mathrm{m^2\,s^{-1}}$ in regions of smooth topography. Enhanced mixing in deeper regions has also been inferred recently by Naviera Garabato *et al.* (2004) who suggest that the widespread, enhanced mixing at depths >500–1000 m in the Southern Ocean is facilitated by bottom-generated internal waves propagating upwards following their generation by the interaction of tidal or geostrophic flows with rough topography. The mixing inferred is supposed to offer a potential contribution to the closure of the MOC. In contrast, Greenland Sea Deep Water is considered to be warmed by inferred mean diapycnal diffusivities of $K_z = 1.2 \times 10^{-3}\ \mathrm{m^2\,s^{-1}}$ across the 2000 m isobath throughout the whole basin in regions *not* confined to rough topography but due to the resonant breakdown of semidiurnal tidal waves at their critical latitude (Walter, 2004). The interesting factor in the FSC is that there is no apparent rough topography which would generate internal waves in the deeper reaches of the channel, nor is it near the critical latitude for internal tides at the semidiurnal frequency. It is thus unclear what the cause of the enhanced diffusivities are at present.

Hansen *et al.* (2001) propose that the intensity of the Faeroe Bank channel overflow has been reduced since 1950 as the density of the bottom waters in the Faeroe Bank Channel, and thus the Faeroe-Shetland Channel, has decreased. As Turrell *et al.* (1999) indicate, below 600 m depth in the FSC a layer of Norwegian Sea/Arctic Intermediate Water (NS/AIW) overlies the Faeroe-Shetland Channel Bottom Water (FSCBW), with the typical transition between the two water masses at approximately 800 m. The density of the FSCBW is variable however and presumably dependent on the degree of mixing that occurs between the FSCBW and NS/AIW; thus enhanced diffusivities in the lower parts of the FSC are obviously consistent with the notion of the mixing and homogenization of the water below the permanent pycnocline and thus the decrease in its density. The consequences of such an effect are the reduced supply of dense water to the North Atlantic Deep Water and eventually a reduced intensity of the MOC from the Faeroe Bank Channel overflow component.

5. Conclusions

We have considered the distribution of density, the rate of dissipation of turbulent kinetic energy, the vertical diffusivity, and the optical backscatter within the Faeroe-Shetland Channel employing a range of observational techniques. Cross-channel transects during which vertical profiles were taken reveal several identifiable mixing regimes which bear significant resemblance to other regions of confined topography and boundary currents.

Mixing in the permanent pycnocline (PP) occurs in discrete patches which are associated with alternating layers of elevated shear magnitude of 20–50 m vertical extent, persistent on timescales of ≤6 hours. The layers are most likely associated with high wavenumber, low frequency internal waves. Whilst it is not presently known what the generation mechanism for such waves is, two likely candidates are the geostrophic adjustment of the slope current over the Shetland slope and the generation of the internal tide which forms an unfocussed web upon repeated reflection. The former mechanism has been previously observed in similar boundary regions and is proposed to be typical of strong boundary currents flowing along continental slopes. With respect to internal tides, there is no spatially distinct evidence of beams of enhanced shear or turbulence emanating from the slope. The localized nature of mixing patches within the interior is however consistent with modeling results which suggest that the superposition of small-scale internal waves resulting from scattering of energy upon reflection of the internal tide results in patches of enhanced mixing. Distinct beams of enhanced optical backscatter extend upwards and away from the Shetland slope into the interior however, and correspond well with the path of the internal tide characteristics emanating from the Shetland slope. In addition to two bottom nepheloid layers at 650 m and 900 m, an intermediate nepheloid layer is also observed to extend horizontally up to 19 km away from the slope, indicating that vigorous mixing over the Shetland slope is effective at resuspending material and that this material is then advected into the interior along isopycnals.

Vertical diffusivities, K_z, in the Faeroe-Shetland Channel are high outside the PP but turbulent buoyancy fluxes are low due to the weak stratification found particularly in the deeper parts of the channel. In the PP the comparatively strong stratification maintains moderate $K_z \approx O(10^{-4.5}\ \mathrm{m^2\ s^{-1}})$, raised by an order of magnitude in the turbulent patches. In the weakly stratified core of the slope current over the Shetland slope and the deep interior of the FSC, $K_z > O(10^{-3}\ \mathrm{m^2\ s^{-1}})$ but the low turbulent buoyancy fluxes imply a negligible exchange of water mass properties across the PP which separates poleward flowing, warm Atlantic waters from the deep Nordic waters returning equatorward. The most vigorous mixing the FSC is found in the bottom boundary layers (BBL) which exhibit elevated turbulence, $\varepsilon > 10^{-8}\ \mathrm{W\ kg^{-1}}$ and $K_z \approx O(10^{-2}\ \mathrm{m^2\ s^{-1}})$. The BBL may be divided into homogenous, or weakly stratified, bottom boundary layers (HBBL) and turbulent stratified boundary layers (TSL). Mixing in HBBLs is achieved through a variety of processes including solibore propagation and convective instabilities arising from the asymmetric response of the BBL to the along-isobath semi-diurnal tidal

flow. TSLs are found immediately above the HBBL and are characterized by an increase in stratification but also shear which is sufficient to lower $Ri < 1$.

In a mean sense the FSC does not contribute significantly to oceanic mixing because the processes that elevate turbulence in the near-bed region where the strongest turbulence is observed occur on relatively short timescales. Solibore propagation occurs approximately every 4 days and with a duration of <4 hours whilst mixing due to the asymmetric response of the BBL lasts for a small fraction of the tidal cycle. Away from boundaries, the weakly stratified interior exhibits high vertical diffusivities but low turbulent buoyancy fluxes, whilst the enhanced stratification in the PP inhibits vertical diffusivities except for the spatially confined and sporadic mixing patches which only periodically elevate mixing.

Acknowledgments. The data were acquired during the Processes on the Continental Slope (PROCS) project, funded by the Netherlands Organization for the Advancement of Scientific Research (NWO). We thank the Department of Sea Technology for the preparation of the moorings and the crew of the RV *Pelagia* for their assistance in the deployment and recovery. We further thank Theo Hillebrand for his careful and thorough preparation of the instrumentation.

APPENDIX

1. Thorpe scales

Vertical profiles obtained from the raw 24 Hz CTD data may be used to infer turbulent mixing rates in horizontally homogeneous flows in which vertical density inversions are the result of turbulent stirring and where the mean horizontal density gradient is much smaller than the vertical gradient. The Thorpe displacement, d_T (Thorpe, 1977), is the vertical distance a parcel of water must be moved in order to rearrange a measured vertical density profile in which density inversions occur into one that is statically stable. The Thorpe scale is defined as the r.m.s value of d_T, and defines the boundaries of a turbulent patch (Moum, 1996; Smyth *et al.,* 2001). Only periods during the profiles when pressure is increasing are considered to eliminate the appearance of false overturns by vertical movement of the instrument by ship motion whilst corrections are made to account for sensor misalignment, the time constants of the sensors and the expansion coefficient of the conductivity cell. It then follows from the relationship $L_o = 0.8L_T$ (Dillon, 1982), where $L_o = (\varepsilon/N^3)^{0.5}$ is the Ozmidov scale which represents the largest scale that can overturn in a stratified flow where the buoyancy force is the same order of magnitude as the inertial forces (Ozmidov, 1965), that $\varepsilon_{(LT)} \equiv N^3(4L_T/5)^2$. For the current study the estimates of ε are then averaged into 20 m vertical blocks.

2. FLY II microstructure probe

The FLY II microstructure probe (Dewey *et al.,* 1987) measures turbulent velocity fluctuations throughout the water column at a sampling rate is 280 Hz as it free falls on a loose tether to the bottom with an approximate speed of 1 m s^{-1}. The estimate of the turbulent shear depends on the fall speed, W, the shear channel gain, G, the calibrated shear probe sensitivity, S, and the output voltage, V_o, (Crawford, 1976) by;

$$\frac{\partial u}{\partial z} = \frac{1}{W}\frac{\partial u}{\partial t} = \frac{V_o}{G2\sqrt{2}\,SW^2}, \tag{7}$$

The turbulent fluctuations, $\partial u/\partial z$, are isolated from the mechanical vibrations and the effects of any vortex shedding from the probe guard by extrapolating the observed shear spectrum of 280 data points $\approx$ 1 second of data assuming a constant fall speed, to the empirical Nasmyth spectrum and neglecting energy at spectral peaks that depart from the theoretical spectrum. The shear variance is then found by integrating the power spectrum. On the assumption of isotropic turbulence the rate of dissipation of turbulent kinetic energy, ε, is then calculated as (Osborn, 1980);

$$\varepsilon = 7.5\mu\left\langle\left(\frac{\partial u}{\partial z}\right)^2\right\rangle \quad (\mathrm{m^2\ s^{-3}}), \tag{8}$$

where the angle brackets denote spatial averaging over a suitable vertical distance, typically ~1 m. The factor 7.5 results from the assumption of isotropic turbulence when measuring a single shear component by the FLY. The assumption of isotropic turbulence is satisfied at dissipation scales in unstratified conditions for large Reynolds numbers (>2000), $\mathrm{Re} = ul/\mu$, where u and l are representative velocity and scales respectively and $\mu = 1.049 \times 10^{-6}\ \mathrm{m^2\ s^{-1}}$ is the kinematic viscosity of seawater (Gargett *et al.,* 1984). In stratified conditions $\varepsilon/\nu N^2 > 200$ is required for isotropy and $\varepsilon/\nu N^2 > 16$ for non-zero buoyancy flux (Gargett *et al.,* 1984). Our observations indicate that turbulence may be assumed to be isotropic outside the permanent pycnocline but that within the stronger stratification are found regions $16 < \varepsilon/\nu N^2 < 200$ (shaded grey, Fig. 12). In such patches turbulence is not truly isotropic due to the suppression of the vertical turbulent fluctuations by the vertical density stratification; thus the factor 7.5 in Eq. (8) overestimates ε by as much as a factor 3.75. In all cases except a patch at 800 m depth over the Faeroe side of the channel however, $\varepsilon/\nu N^2 > 16$ as required for nonzero buoyancy flux. The noise level of the FLY is $\varepsilon = 2 \times 10^{-9}\ \mathrm{W\ kg^{-1}}$.

3. 'Direct' and 'indirect' estimates of ε and K_z

We compare here estimates of K_z made using ε as determined from the FLY data (the 'direct' method, designated as K_z (FLY)), and from the CTD measurements by using L_T (the 'indirect' method, designated by K_z (L_T)). In both methods K_z is estimated by (6) assuming $\Gamma_o = 0.2$.

Comparison is made for the eight stations conducted over the slope in the vicinity of the LR-ADCPs. Estimates of ε and K_z derived from L_T are averaged over 20 m intervals and so the FLY data, of ~1 m resolution, are block-averaged over matching 20 m intervals. The ratio $R = [K_Z\,(L_T)]/[K_Z\,(\mathrm{FLY})]$ is calculated for each pair of samples determined by the two methods and the mean ratio, R_{mean}, for each pair of profiles determined for those points for which $10^1 > R > 10^{-1}$. During PROCS-1, 86% of the data points fall within this arbitrary threshold (Fig. 13a), the proportion falling to 78% during PROCS-3 (Fig. 13b). Of those points within the threshold, $R > 1$ for all profiles (except one during

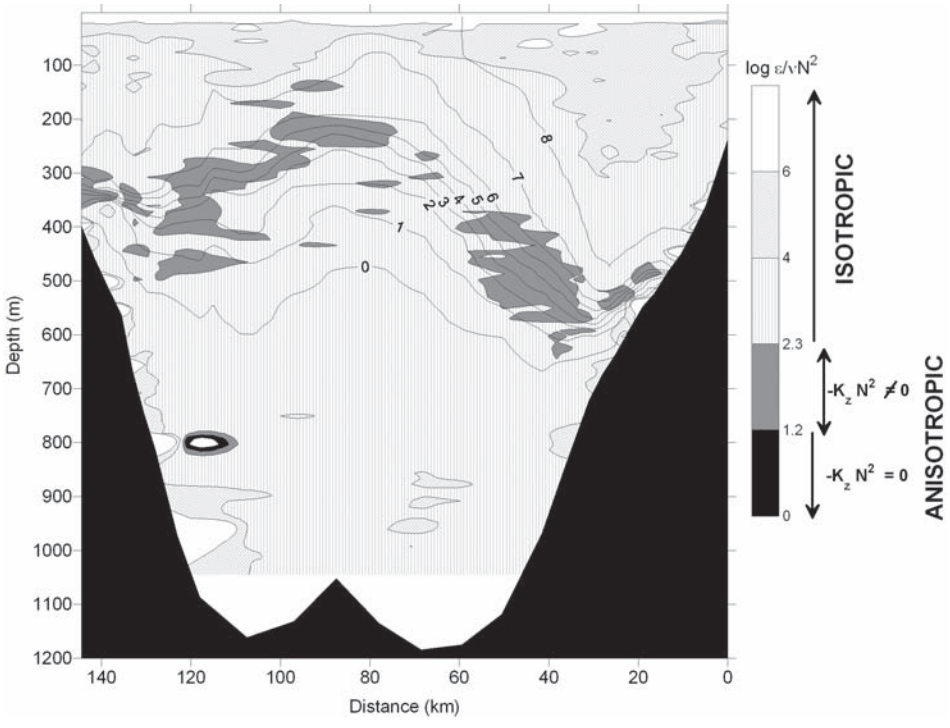

Figure 12. Cross-channel transect of $\log_{10}(\varepsilon/\nu N^2)$ during P1-T1. ε and N^2 were sampled by the FLY and CTD, respectively, as in Figures 3 and 4 and the kinematic viscosity, ν, by the CTD. Regions where $\varepsilon/\nu N^2 < 200$ (anisotropic turbulence) are shaded grey where $\varepsilon/\nu N^2 > 16$, required for nonzero buoyancy flux (Gargett et al., 1984), and black where $\varepsilon/\nu N^2 < 16$.

PROCS-3 when $R = 0.6$), with $R_{\text{mean}} = 1.3$ and 2.2 for the two respective cruises (dashed line in Fig. 1); thus K_Z (L_T) tends to be larger than K_Z (FLY), on average by a factor of approximately 2.

During both cruises the standard deviation of R increased by a factor of 2 during the profiles conducted immediately following a storm, after ε increased throughout the entire water column and with a large degree of variability in the vertical. Estimates of ε from the CTD profiles were also elevated following the storm however, indicating genuine overturns and giving confidence that the increased levels of ε measured by the FLY were due to turbulence rather than instrument noise. Prior to the storms however, constant background values of $\varepsilon \approx 2 \times 10^{-9}$ W kg^{-1} measured by the FLY represent the noise level of the instrument whilst the lower estimates made by the CTD of $\varepsilon \approx 5 \times 10^{-10}$ W kg^{-1} are more indicative of genuine oceanic background values of $\varepsilon \approx O(10^{-10})$ W kg^{-1}. During P1-T1 however only 0.001% of the ε_{FLY} samples fell below the noise level of the instrument.

Estimates of K_Z (L_T) are less reliable in the very weakly or strongly stratified parts of the water column; all estimates when $N^2 > 10^{-4}$ s^{-2} (crosses in Fig. 13) are more than one

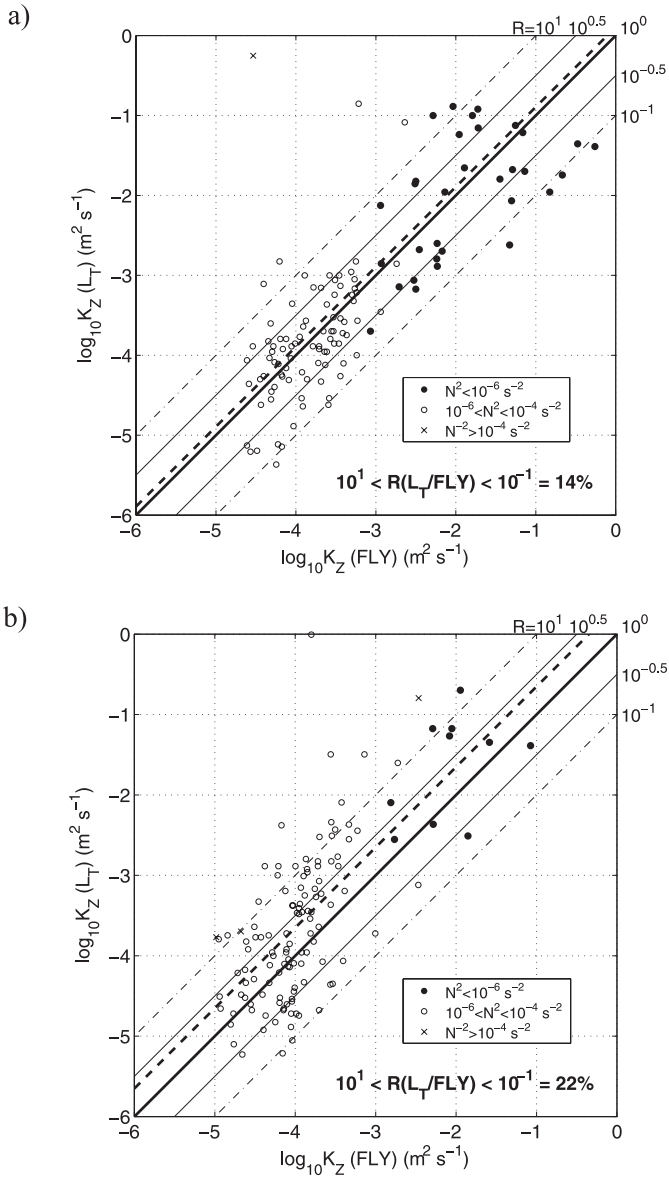

Figure 13. Vertical diffusivities during (a) PROCS-1, and (b) PROCS-2 derived from Thorpe scales (K_Z (L_T)) calculated from CTD profiles against those calculated directly from FLY velocity microstructure profiles (K_Z (FLY)). Black dots (●) correspond to regions of weak stratification where $N^2 < 10^{-6}\,\mathrm{s}^{-2}$, circles (○) to moderate stratification where $10^{-6} < N^2 < 10^{-4}\,\mathrm{s}^{-2}$, and crosses (×) to strong stratification where $N^2 > 10^{-4}\,\mathrm{s}^{-2}$. The solid diagonal line represents a ratio of 1 : 1 for estimates of K_Z derived from the two methods, the thin solid lines to a ratio of $\pm 1 : 10^{0.5}$ and the dot-dashed lines to $\pm 1 : 10$. The dashed line represents the mean ratio of the points whose ratios lie within one order of magnitude, whilst the number of points which fail to do so are indicated in the bottom right of each panel. Of the total number of points whose ratios lie within an order of magnitude of each other, the percentage of the total falling within each ratio band of magnitude $10^{0.5}$ is given.

order of magnitude larger than those made with the FLY probe and provide unrealistically large values of K_Z. The likely reason for this is the imperfect corrections applied to the short-term mismatch of the salinity and temperature sensor responses and to the thermal lag of the conductivity cell, resulting in spuriously large overturns being detected. The standard deviation of R in weakly stratified regions ($N^2 < 10^{-6}$ s^{-2}) is a factor of 2 higher than those in moderately stratified conditions during both cruises. The weakness of the stratification in the interior of the FSC implies a large sensitivity of the overturns to the background density gradient during the reordering process. The larger scatter of K_Z (L_T) is thus a consequence of the reduction in instrument accuracy relative to the background N.

REFERENCES

Alford, M. H. and R. Pinkel. 2000. Observations of overturning in the thermocline: The context of ocean mixing. J. Phys. Oceanogr., *30,* 805–832.

Bunt, J. A. C., P. Larcombe and C. F. Jago. 1999. Quantifying the response of optical backscatter devices and transmissiometers to variations in suspended particulate matter. Cont. Shelf Res., *19,* 1199–1220.

Cahn, A. 1945. An investigation of the free oscillations of a simple current system. J. Meteor., *2,* 113–119.

Crawford, W. R. 1976. Turbulent energy dissipation in the Atlantic Equatorial Undercurrent. PhD thesis, University of British Columbia, 150 pp.

——1986. A comparison of length scales and decay times of turbulence in stably stratified flows. J. Phys. Oceanogr., *16,* 1847–1854.

Dewey, R. K., W. R. Crawford, A. E. Gargett and N. S. Oakey. 1987. A microstructure instrument for profiling oceanic turbulence in coastal bottom boundary layers. J. Atmos. Ocean. Tech., *4,* 288–297.

Dillon, T. M. 1982. Vertical overturns: A comparison of Thorpe and Ozmidov length scales. J. Geophys. Res., *87* (C12), 9601–9613.

Gargett, A. E. and J. N. Moum. 1995. Mixing efficiencies in turbulent tidal fronts: Results from direct and indirect measurements of density flux. J. Phys. Oceanogr., *25,* 2583–2608.

Gargett, A. E., T. R. Osborn and P. R. Nasmyth. 1984. Local isotropy and the decay of turbulence in a stratified fluid. J. Fluid Mech., *144,* 231–280.

Garrett, C. and W. Munk. 1979. Internal waves in the ocean. Ann. Rev. Fluid Mech., *11,* 339–369.

Gerkema, T. 2001. Internal and interfacial tides: Beam scattering and local generation of solitary waves. J. Mar. Res., *59,* 227–255.

Gordon, L. E. and J. M. Huthnance. 1987. Storm-driven continental shelf waves over the Scottish continental shelf. Cont. Shelf Res., *7,* 1015–1048.

Hansen, B., W. R. Turrell and S. Østerhus. 2001. Decreasing overflow from the Nordic Seas into the Atlantic Ocean through the Faeroe Bank channel since 1950. Nature, *411,* 927–930.

Hopkins, T. S. 1991. The GIN sea: a synthesis of its physical oceanography and literature, 1972–1985. Earth Sci. Rev., *30,* 175–318.

Hosegood, P., J. Bonnin and H. van Haren. 2004. Solibore-induced sediment resuspension in the Faeroe-Shetland Channel. Geophys. Res. Lett., *31,* L09301, doi:10.1029/2004GL019544.

Hosegood, P. J. and H. van Haren. 2003. Ekman-induced turbulence over the continental slope in the Faeroe-Shetland Channel as inferred from spikes in current meter observations. Deep-Sea Res. I, *50,* 657–680.

——2004. Near-bed solibores over the continental slope in the Faeroe-Shetland Channel. Deep-Sea Res. II, *51,* 2943–2971.

Howe, J. A., M. S. Stoker, D. A. V. Stow and M. C. Akhurst. 2002. Sediment drifts and contourite

sedimentation in the northeastern Rockall Trough and Faeroe-Shetland Channel, North Atlantic Ocean, *in* Deep-Water Contourite Systems: Modern Drifts and Ancient Series, Seismic and Sedimentary Characteristics, D. Stow, C. J. Pudsey, J. A. Howe, J. C. Faugeres, A. R. Viana, eds., Geological Society, London, Memoirs, *22,* 65–72.

Huthnance, J. M. 1986. The Rockall slope current and shelf edge processes. Proc. Roy. Soc. Edin., *88B,* 83–101.

Kuo, A. C. and L. M. Polvani. 1997. Time-dependent fully nonlinear geostrophic adjustment. J. Phys. Oceanogr., *27,* 1614–1634.

LeBlond, P. H. and L. A. Mysak. 1978. Waves in the Ocean, Elsevier Scientific Publishing Company, Amsterdam.

Lien, R. C. and M. C. Gregg. 2001. Observations of turbulence in a tidal beam and across a coastal ridge. J. Geophys. Res., *106,* 4575–4391.

Lueck, R. G. and T. D. Mudge. 1997. Topographically induced mixing around a shallow seamount. Science, *276,* 1831–1833.

Maas, L. R. M., D. Benielli, J. Sommeria and F-P. A. Lam. 1997. Observation of an internal wave attractor in a confined, stably stratified fluid. Nature, *388,* 557–561.

Miles, J. 1987. Richardson's number revisited, *in* Preprints of 3rd Intl. Symposium on Stratified Flows, CalTech, Pasadena, CA, February 3–5, 1–7.

Mooers, C. N. K. 1973. Several effects of a baroclinic current on the cross-stream propagation of inertial-internal waves. Geophys. Fluid Dyn., *6,* 245–275.

Moum, J. 1996. Efficiency of mixing in the main thermocline. J. Geophys. Res., *101*(C5), 12,057–12,069.

Moum, J. N., D. R. Caldwell, J. D. Nash and G. D. Gunderson. 2002. Observations of boundary mixing over the continental slope. J. Phys. Oceanogr., *32,* 2113–2130.

Naveira Garabato, A. C., K. L. Polzin, B. A. King, K. J. Heywood and M. Visbeck. 2004. Widespread intense turbulent mixing in the Southern Ocean. Science, *303,* 210–213.

Oey, L. Y. 1998. Eddy energetics in the Faroe-Shetland channel: a model resolution study. Cont. Shelf Res., *17,* 1929–1944.

Osborn, T. R. 1980. Estimates of the local rate of vertical diffusion from dissipation measurements. J. Phys. Oceanogr., *10,* 83–89.

Ozmidov, R. V. 1965. On the turbulent exchange in a stably stratified ocean. Izvestiya, Acad. Sci. U.S.S.R., Atmos. Ocean. Phys., *1,* 861–871.

Pingree, R. D. and A. L. New. 1991. Abyssal penetration and bottom reflection of internal tidal energy in the Bay of Biscay. J. Phys. Oceanogr., *21,* 28–39.

Prinsenberg, S. J., W. L. Wilmot and M. Rattray. 1974. Generation and dissipation of coastal internal tides. Deep-Sea Res., *21,* 263–281.

Rainville, L. and R. Pinkel. 2004. Observations of energetic high-wavenumber internal waves in the Kuroshio. J. Phys. Oceanogr., *34,* 1495–1505.

Rohr, J. and C. Van Atta. 1987. Mixing efficiencies in stably stratified growing turbulence. J. Geophys. Res., *92,* 5481–5488.

Saunders, P. M. 1990. Cold outflow from the Faeroe Bank Channel. J. Phys. Oceanogr., *20,* 29–43.

Sherwin, T. J. 1988. Analysis of an internal tide observed on the Malin Shelf, north of Ireland. J. Phys. Oceanogr., *18,* 1035–1050.

Sherwin, T. J., W. R. Turrell, D. R. G. Jeans and S. Dye. 1999. Eddies and a mesoscale deflection of the slope current in the Faroe-Shetland Channel. Deep-Sea Res. I, *46,* 415–438.

Smyth, W. D., J. N. Moum and D. R. Caldwell. 2001. The efficiency of mixing in turbulent patches: Inferences from direct simulations and microstructure observations. J. Phys. Oceanogr., *31,* 1969–1992.

Thorpe, S. A. 1975. Excitation, dissipation and interaction of internal waves in the deep ocean. J. Geophys. Res., *80,* 328–338.

——1977. Turbulence and mixing in a Scottish Loch. Phil. Trans. Roy. Soc. Lond., *286,* 125–181.

——1999. The generation of alongslope currents by breaking internal waves. J. Phys. Oceanogr., *29,* 29–38.

Turrell, W. R., G. Slesser, R. D. Adams, R. Payne and P. A. Gillibrand. 1999. Decadal variability in the composition of Faeroe-Shetland Channel Bottom Water. Deep-Sea Res. I, *46,* 1–25.

van Haren, H. 2000. Properties of vertical current shear across stratification in the North Sea. J. Mar. Res., *58,* 465–491.

——2004. Some observations of nonlinearly modified internal wave spectra. J. Geophys. Res., *109,* C03045, doi:10.1029/2003/JC002136.

van Haren, H., L. Maas, J. T. F. Zimmerman, H. Ridderinkhof and H. Malschaert. 1999. Strong inertial currents and marginal internal wave stability in the central North Sea. Geophys. Res. Lett., *26,* 2993–2996.

Walter, M. 2003. Warming of the Greenland Sea Deep Water induced by abyssal mixing. PhD thesis, University of Bremen, 132 pp.

Winkel, D. P., M. C. Gregg and T. B. Sanford. 2002. Patterns of shear and turbulence across the Florida Current. J. Phys. Oceanogr., *32,* 3269–3285.

Yamazaki, H. and T. R. Osborn. 1993. Direct estimation of heat flux in the seasonal thermocline. J. Phys. Oceanogr., *23,* 503–516.

Received: *22 July, 2004;* revised: *18 January, 2005.*